THE ASTROPHYSICAL JOURNAL, 375:46–68, 1991 July 1

OPTICAL POLARIZATION OF A COMPLETE SAMPLE OF RADIO SOURCES

C. D. IMPEY
Steward Observatory, University of Arizona, Tucson, AZ 85721
C. R. LAWRENCE
Owens Valley Radio Observatory and Palomar Observatory, California Institute of Technology, Radio Astronomy 105-24, Pasadena, CA 91125
AND
S. TAPIA
Steward Observatory, University of Arizona; and MIT–Lincoln Laboratories, Lexington, MA 02173
Received 1990 August 29; accepted 1990 December 21

ABSTRACT

Polarimetry of 50 strong radio sources is presented and combined with VLBI observations and optical spectroscopy in a study of the radio and optical properties of a complete 5 GHz sample. The sample is almost equally divided into radio galaxies and quasars. High polarization ($p > 3\%$) is strongly correlated with the fraction of the total 5 GHz flux density found in a milliarcsecond core (F_c). The fraction of sources with high polarization rises from 13% for sources with $F_c < 0.1$ to 45% for sources with $F_c > 0.1$. Few radio galaxies contain optical cores with high polarization, but the detection rate of such cores is consistent with the hypothesis that *all* radio sources contain optically polarized cores, with strength proportional to the core radio flux density. Two-thirds of the known superluminal sources in the sample have high polarization. High optical polarization, optical power-law fraction, line-to-continuum ratio, emission lines of small equivalent width, and large amplitude flux variability are all strongly correlated with the fraction of the 5 GHz radio flux density that is unresolved on VLBI scales. The distributions of these optical properties are well matched by a model where the radio and optical radiation have the same beaming geometry, and with Doppler boosting of a factor of 10–100 in the optical. We confirm in this complete sample a striking alignment of the position angle of the VLBI structure axis and the position angle of optical polarization in highly polarized sources. We also find that the highly polarized sources have a large amount of *mis*alignment between the VLBI structure axis and the axis of large-scale radio structure. The properties of weak-lined objects are consistent with the hypothesis that such objects are of two kinds: sources with high isotropic radio and line luminosity and large γ, viewed at an angle to the line of sight much less than $1/\gamma$; and sources of low isotropic radio and line luminosity and moderate γ, viewed at $\sim 1/\gamma$ to the line of sight. Various properties of core-dominated sources require a beaming model with a range of Lorentz factors.

Subject headings: BL Lacertae objects — galaxies: nuclei — polarization — quasars — radio sources: galaxies

1. INTRODUCTION

Observations of compact radio sources address the central issue in research on active galactic nuclei, the nature of the power source. The central object remains mysterious, but the evidence that continuum radiation is relativistically boosted is accumulating. The most persuasive evidence comes from radio observations using the technique of very long baseline interferometry (VLBI). At typical VLBI resolution of $\sim 0\farcs001$, most compact radio sources show cores and one-sided jets. Knots in the jets often have proper motions that, if interpreted naively, would imply superluminal transverse motion of the radio-emitting plasma. In the standard interpretation, material ejected from the nucleus is collimated on scales of less than 1 pc and is moving at close to the speed of light along a path close to the line of sight (Kellermann & Pauliny-Toth 1981; Pearson & Zensus 1987). Radiation from relativistic plasma is highly anisotropic, and the intensity in the direction of motion can be orders of magnitude greater than the average over a sphere. Thus the appearance of a source with relativistic components must depend dramatically on the direction from which it is seen. Apparent superluminal motion is common among compact radio sources (Pearson & Readhead 1988; Witzel et al. 1988).

Indirect arguments for relativistic source motion have been derived from infrared, optical, and X-ray observations. These spectral regions contain most of the energy output of strong radio sources. The fact that large Compton-scattered X-ray fluxes are not observed in these sources is easily explained by the effects of relativistic motion (Marscher et al. 1979; Cohen 1989). Direct VLBI measurements of brightness temperature, as well as intrinsic flux variability timescales, show that the Compton limit is exceeded in many sources (Linfield et al. 1989; Witzel 1990; Quirrenbach & Witzel 1990). Infrared luminosities can vary on time scales that are shorter than the light-crossing time for an Eddington-limited gravitational power source (Impey et al. 1982). The energy distributions of compact radio sources are often strikingly simple, with one synchrotron component from millimeter to ultraviolet wavelengths (Landau et al. 1986). The evidence for synchrotron emission is based on the widespread existence of rapid variability and high polarization.

There is a strong statistical link between compact radio emission and polarized, variable optical emission. The term "blazar" has been coined for such sources (Angel & Stockman 1980); the definition includes highly polarized quasars as well as objects with low-luminosity emission lines such as BL

Lacertae (Moore & Stockman 1981). Most compact radio sources are associated with high-luminosity quasars, although there are a number of radio galaxies with compact cores. Recent surveys have found many examples of compact radio sources with blazar properties (Fugmann & Meisenheimer 1988; Kühr & Schmidt 1989; Wills 1989; Impey & Tapia 1990). Impey & Tapia (1990) found that the fraction of radio quasars with high optical polarization increases smoothly with increasing compactness of the radio emission. Virtually every source with more than half the total flux density in an unresolved VLBI core is highly polarized. These are also the sources most likely to show superluminal motion; over 70% of the confirmed superluminal sources have blazar properties (Impey 1987). Moreover, there is an intriguing alignment between the VLBI structure axis and the preferred position angle of polarization (Rusk & Seaquist 1985; Impey 1987).

Theorists have argued persuasively that both the radio and optical data indicate incoherent synchrotron radiation by jetlike structures aligned close to the observer's line of sight (Blandford & Rees 1978; Blandford & Königl 1979). The inevitable consequences of relativistic motion neatly account for the lack of self-Compton X-rays, the rapid flux variability, and apparently superluminal transverse motion. So-called beaming models have been pursued in two ways. First, it has been recognized that simple ballistic models are idealized versions of what in reality may be a complex hydrodynamic flow (Lind & Blandford 1985). Doppler flux boosting is so dramatic that the observed emission may come from a tiny fraction of the jet volume (Phinney 1985). Second, the compact or core-dominant sources form a small percentage of all known active galactic nuclei. The vast majority have extremely weak radio emission and no evidence for relativistic motion. An attractive generalization of the beam model proposes that high-luminosity radio sources all have relativistic jets, and that the observed differences between powerful radio galaxies and quasars, and between flat and steep spectrum radio sources are caused by Doppler boosting and projection effects (Orr & Browne 1982; Scheuer 1987; Barthel 1989).

Only complete samples selected on the basis of isotropic radiation can provide adequate tests of beaming models. There are only two spectral regions where isotropy is almost certain, namely, below ~ 500 MHz (rest frame), where high-brightness-temperature beamed components are self-absorbed, and in the far-infrared (~ 60–100 μm rest) where low-temperature dust emission peaks. However, IR selection is complicated by the fact that both nuclear synchrotron emission, possibly Doppler boosted, and emission from nonnuclear dust associated with star formation may dominate the isotropic IR emission from the nucleus.

Samples selected at high radio frequencies cannot be used to establish parent populations or to test beaming models directly; however, for the purpose of studying the characteristics of beamed sources they are extremely valuable. The best-studied high-frequency sample is a flux density-limited sample of 65 extragalactic radio sources selected at 5 GHz by Pearson & Readhead (1981). First epoch VLBI maps have now been published for this sample (Pearson & Readhead 1988), and second and third epoch observations have been reduced. High-quality optical spectra have been obtained for all 65 sources, with early results published by Lawrence et al. (1986, 1987). In this paper, we present new optical polarimetry for 50 sources from the complete sample. The observations are described in § 2, and the polarization properties of radio galaxies and quasars are summarized in §§ 3 and 4. The global properties of the optical and radio emission are discussed in § 5. Constraints on relativistic beaming models are considered in § 6, and a summary of this work follows in § 7. This is the first time that VLBI observations and optical polarimetry and spectroscopy have been accumulated for a large sample of compact radio sources.

2. OBSERVATIONS

The 65 radio sources in the VLBI sample are selected according to the following criteria: $\delta > 35°$; $b^{II} > 10°$; and $S_{5\,\mathrm{GHz}} > 1.3$ Jy. (One of the sources is the nearby starburst galaxy M82, whose radio luminosity, from a large number of supernova remnants rather than central activity, is by far the lowest in the sample. It is dissimilar to the compact and mostly high luminosity radio sources discussed in this paper). Optical polarimetry for 50 of the radio sources was obtained using the MINIPOL polarimeter on the Hale 200 inch (5 m) telescope on Palomar Mountain. Repeat measurements were made for 13 of the sources. The remaining 15 radio sources are mostly faint galaxies for which accurate polarimetry would be extremely difficult. All the data were acquired during three observing runs: 1986 July 13–14, 1986 December 22–24, and 1987 April 4–6. The observations were made through a 1.″3 aperture, in good weather conditions with seeing in the range 1″–1.″5. A description of the instrument and the calibration procedures used for each night of observation can be found in Dolan & Tapia (1986). Typical levels of accuracy and repeatability of MINIPOL for faint sources are given by Impey, Malkan, & Tapia (1989). Polarization errors for faint radio sources are limited by photon statistics. The observations were made unfiltered; the spectral band defined by the sensitivity of the GaAs phototubes is 3200–8800 Å. For the energy distribution of a typical radio source, the effective wavelength of the polarization measurement is ~ 5700 Å.

Table 1 lists the complete VLBI sample, with polarimetry from this paper and additional previously published data. The degree of polarization has been corrected for low signal-to-noise-ratio bias, according to the prescription of Simmons & Stewart (1985). This paper will use a simple division of sources into high ($p > 3\%$) and low ($p < 3\%$) polarization. We note that the distinction between observed and debiased polarization is small for sources with $p > 3\%$ and $p/\sigma(p) > 3$. Only two sources with $p > 3\%$ have a polarization error large enough that the 95% confidence interval includes zero polarization (0040+517 and 0605+480). On the basis of one noisy measurement, these cannot be claimed as highly polarized sources. The literature search for previous polarimetry was extensive but not necessarily complete; references are presented in the footnotes to Table 1.

This set of radio sources is the largest complete sample with comprehensive VLBI data, optical spectroscopy and optical polarimetry. Based on optical morphology alone, 30 of the 65 are "galaxies" and the remaining 35 are stellar objects, which we will refer to as "quasars." Redshifts are known for 60 sources (92%). Polarimetry is 89% complete for the quasars, and 67% complete for the galaxies. All but one of the galaxies without polarimetry are fainter than $V = 20$ mag, so the polarimetry is strongly biased toward optically bright galaxies. The quasar polarimetry is complete enough to be virtually immune to selection effects. For nearly half the sample, our new polarization measure is the only published value. For the rest, the sampling of polarization is extremely nonuniform. Six

TABLE 1

OPTICAL POLARIMETRY

Source (1)	(2)	z (3)	$S_{5\,\mathrm{GHz}}$ (4)	M_V (5)	ID (6)	b^{II} (7)	$p \pm \sigma_p$(%) (8)	$\theta \pm \sigma_\theta$ (9)	UT Date (10)	$p_{\max}$(%) (11)	N_{obs} (12)	Ref (13)
0016+731		1.781	1.65	18.0	Q	+10.7	0.9 ± 0.7	108 ± 17	86/12/22	0.9	1	1
0040+517	3C 20	0.174	4.18	19.0	G	−10.8	5.0 ± 2.1	46 ± 10	86/12/24	5.0	1	1
0108+388		...	1.35	22.0	G	−23.6	...	...	...	...	...	...
0133+476		0.849	3.26	19.0	Q	−14.3	20.8 ± 0.7	67 ± 1	86/12/22	20.8	1	1
0153+744		2.338	1.51	17.0	Q	+12.4	1.1 ± 0.3	106 ± 7	86/12/22	1.1	1	1
0210+860	3C 61.1	0.184	1.68	21.0	G	+23.7	...	...	...	...	...	...
0212+735		2.367	2.20	19.0	Q	+12.0	0.7 ± 2.6	...	86/12/22	7.8	2	2
0220+427	3C 66B	0.0215	3.75	12.9	G	−16.8	1.1 ± 0.1	106 ± 3	86/12/22	1.1	2	1
0314+416	3C 83.1B	0.0181	3.53	12.5	G	−13.1	0.7 ± 0.1	103 ± 2	86/12/22	0.7	1	1
0316+413	3C 84	0.0172	47.20	11.9	G	−13.3	0.6 ± 0.1	114 ± 3	86/12/22	6.0	52	3
0404+768	4C 76.03	...	2.79	22.0	G	+18.3	...	...	...	...	...	...
0454+844		...	1.40	18.0	Q	+24.7	14.2 ± 3.1	15 ± 6	86/12/11	18.5	2	4
0538+498	3C 147	0.545	8.18	17.8	Q	+10.3	2.3 ± 0.9	169 ± 11	86/12/22	2.3	2	1
0605+480	3C 153	0.277	1.35	18.5	G	+13.4	5.3 ± 4.3	144 ± 19	86/12/24	5.3	1	1
0710+439		0.518	1.66	20.7	G	+22.2	...	...	...	...	...	...
0711+356		1.620	1.51	17.0	Q	+19.7	1.0 ± 1.0	29 ± 24	86/12/24	1.0	1	1
0723+679		0.846	1.31	18.0	Q	+28.4	1.5 ± 1.0	2 ± 16	86/12/22	1.5	2	1
0804+499		1.430	2.07	17.5	Q	+32.6	8.6 ± 0.7	179 ± 2	86/12/24	8.6	1	1
0809+483	3C 196	0.871	4.35	17.8	Q	+33.2	0.8 ± 0.9	9 ± 23	86/12/22	0.8	2	1
0814+425		...	1.68	17.7	Q	+33.4	8.7 ± 1.4	162 ± 5	86/12/22	12.0	4	4
0831+557	4C 55.16	0.242	5.60	17.5	G	+36.6	3.0 ± 1.2	3 ± 11	86/12/24	3.0	1	1
0836+710	4C 71.07	2.170	2.57	16.5	Q	+34.4	1.0 ± 0.5	102 ± 12	86/12/22	1.0	1	1
0850+581	4C 58.17	1.322	1.41	18.0	Q	+38.9	0.4 ± 0.2	164 ± 14	86/12/24	0.4	1	1
0859+470	4C 47.29	1.462	1.78	18.7	Q	+41.6	0.7 ± 0.8	20 ± 22	86/12/24	0.7	1	1
0906+430	3C 216	0.670	1.78	18.5	Q	+42.8	3.8 ± 0.2	53 ± 2	86/12/24	21.0	7	5
0917+458	3C 219	0.174	2.29	17.2	G	+44.8	0.3 ± 0.7	...	86/12/24	0.3	1	1
0923+392	4C 39.25	0.699	8.90	17.9	Q	+46.2	0.4 ± 0.3	116 ± 18	86/12/24	0.9	4	6
0945+408	4C 40.24	1.252	1.39	17.5	Q	+50.3	0.3 ± 0.5	...	86/12/24	0.3	1	1
0951+699	M 82	0.0009	3.94	8.4	G	+40.6	0.9 ± 0.1	39 ± 3	86/12/24	0.9	1	1
0954+556	4C 55.17	0.909	2.27	17.7	Q	+47.9	6.4 ± 0.5	1 ± 2	86/12/24	6.4	1	1
0954+658		0.368	1.46	16.7	Q	+43.1	19.1 ± 0.2	170 ± 1	86/12/24	33.7	4	4
1003+351	3C 236	0.0989	1.32	16.0	G	+54.0	0.2 ± 0.3	...	86/12/24	0.2	2	1
1031+567		0.450	1.31	21.3	G	+51.9	...	...	...	...	...	...
1157+732	3C 268.1	0.970	2.63	21.5	G	+43.6	...	...	...	...	...	...
1254+476	3C 280	0.994	1.53	20.0	G	+69.8	...	...	...	...	...	...
1358+624	4C 62.22	0.431	1.77	20.9	G	+53.1	...	...	...	...	...	...
1409+524	3C 295	0.461	6.48	20.1	G	+60.8	...	...	...	...	...	...
1458+718	3C 309.1	0.905	3.34	16.8	Q	+42.1	1.0 ± 0.4	107 ± 11	86/12/24	1.0	2	1
1609+660	3C 330	0.549	2.35	20.3	G	+40.7	2.8 ± 1.4	126 ± 12	87/04/05	2.8	1	1
1624+416	4C 41.32	2.550	1.31	22.0	Q	+44.2	...	...	...	...	...	...
1633+382	4C 38.41	1.814	4.08	18.0	Q	+42.3	1.1 ± 0.2	114 ± 6	86/07/13	2.6	4	6
1634+628	3C 343	0.988	1.50	20.6	Q	+39.4	...	...	...	...	...	...
1637+574		0.745	1.44	17.0	Q	+40.4	2.4 ± 0.8	170 ± 9	86/07/13	2.4	2	1
1641+399	3C 345	0.595	10.90	16.0	Q	+40.9	11.2 ± 0.2	53 ± 1	86/07/13	35.3	88	7
1642+690	4C 69.21	0.751	1.43	19.2	Q	+36.6	16.6 ± 1.7	8 ± 3	86/07/13	16.6	3	1
1652+398	Mk 501	0.0337	1.42	13.8	G	+38.9	3.0 ± 0.1	125 ± 1	86/07/13	3.6	48	8
1739+522	4C 51.37	1.375	1.99	18.5	Q	+31.7	3.7 ± 0.2	172 ± 2	86/07/13	3.7	2	1
1749+701		...	1.81	17.0	Q	+30.7	10.5 ± 0.2	129 ± 1	86/07/13	11.5	3	9
1803+784		0.680	2.63	17.0	Q	+29.1	7.0 ± 0.2	171 ± 1	86/07/13	35.2	3	4
1807+698	3C 371	0.050	2.33	14.2	G	+29.2	8.0 ± 0.1	106 ± 1	86/07/13	10.0	69	10
1823+568	4C 56.27	0.664	1.67	18.4	Q	+26.1	16.8 ± 0.7	20 ± 1	86/07/13	16.8	4	1
1828+487	3C 380	0.692	6.19	16.8	Q	+23.5	0.2 ± 0.2	...	86/07/13	0.4	2	11
1842+455	3C 388	0.0908	1.77	15.3	G	+20.2	0.4 ± 0.4	151 ± 21	86/07/13	0.4	1	1
1845+797	3C 390.3	0.0569	4.32	15.0	G	+27.1	1.3 ± 0.1	136 ± 3	86/07/13	3.5	47	5
1928+738	4C 73.18	0.302	3.30	16.5	Q	+23.5	1.2 ± 0.1	143 ± 2	86/07/13	1.3	3	1
1939+605	3C 401	0.201	1.52	18.0	G	+17.8	1.1 ± 0.7	59 ± 15	86/07/14	1.4	2	1
1954+513		1.220	1.43	18.5	Q	+11.8	...	...	...	1.5	1	6
2021+614		0.227	2.31	19.5	G	+13.8	0.3 ± 0.3	...	86/07/13	0.3	1	1
2153+377	3C 438	0.292	1.54	19.2	G	−13.0	...	...	...	...	...	...
2200+420	BL Lac	0.0688	4.75	14.5	G	−10.4	13.7 ± 0.1	18 ± 1	86/07/13	23.0	...	5
2229+391	3C 449	0.0171	1.39	13.2	G	−15.9	0.7 ± 0.2	125 ± 6	86/07/13	0.7	4	1
2243+394	3C 452	0.0811	3.26	16.0	G	−17.1	0.2 ± 0.1	85 ± 13	86/07/14	0.2	1	1
2342+821		0.735	1.30	20.5	G	+19.9	...	...	...	...	...	...
2351+456	4C 45.51	2.000	1.41	20.6	Q	−15.8	...	...	...	...	...	...
2352+495		0.237	1.77	19.0	G	−12.0	1.2 ± 2.0	...	86/12/24	1.2	1	1

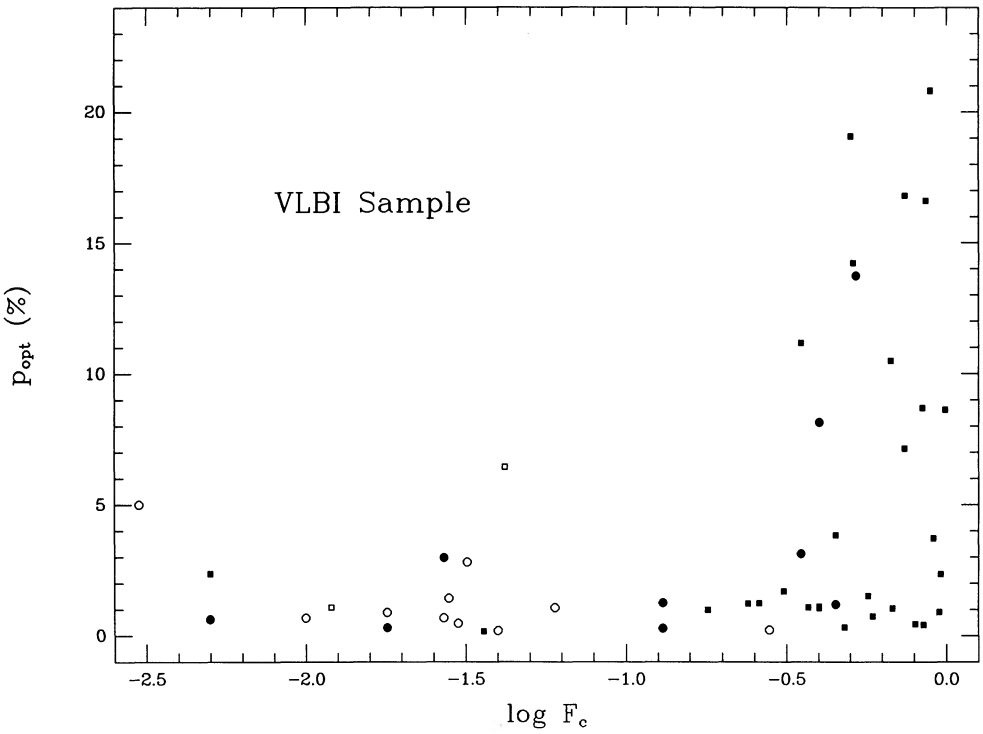

FIG. 1.—First measured value of optical polarization for the entire sample vs. the fraction of the radio flux density in the VLBI core. Circles are radio galaxies and squares are quasars, as identified in Table 1. Open symbols are used for objects with upper limits on F_c.

well-studied sources have dozens of published measurements (3C 84, 3C 345, Mrk 501, 3C 371, 3C 390.3, and BL Lacertae), the rest have only a couple. Clearly, the distribution of the maximum polarization detected in *any* observation, p_{max}, depends on the duty cycle of high- and low-polarization states. Estimates of the duty cycle of quasar polarization have been made by Fugmann & Meisenheimer (1988), Impey & Tapia (1990), and Kühr & Schmidt (1989).

In this paper, we will represent the polarization by the first measured value. This procedure gives unbiased statistics and a reasonable estimate of the behavior of this property for a group of objects. However, compact radio sources often have a highly variable degree and position angle of optical polarization. Therefore, the first measured values of these quantities may not be representative for an individual object.

Figure 1 shows the first recorded measure of optical polarization for the entire sample plotted against F_c, the fraction of the total 5 GHz flux density found in the milliarcsecond core (see notes in Table 2, below). The percentage of sources with high polarization ($p > 3\%$) rises from 7% for objects with $F_c < 0.1$ to 52% for objects with $F_c > 0.1$ (omitting the two radio galaxies with large fractional polarization errors). For galaxies separately, the fractions are 0/11 and 4/7, while for quasars, they are 1/4 and 13/26. Similar proportions are obtained if p_{max} is used rather than the first measured value. Since only upper limits on F_c are known for many sources, we cannot calculate a correlation coefficient between polarization and F_c. However, if we divide the sample at $F_c = 0.1$ and $p = 3\%$, we find the probability that high polarization and radio compactness are not related is 0.0074. In the following two sections, we discuss the properties of the quasars and radio galaxies separately.

3. POLARIZATION IN RADIO GALAXIES

3.1. *Radio Compactness*

Figure 2 shows the first measurement optical polarization plotted against F_c for the galaxies in the sample (circles, omitting 0040+517 and 0605+480 due to their large errors) as well as for galaxies taken from Antonucci (1984) and Rudy et al. (1983), and low-redshift BL Lac objects from Angel & Stockman (1980) (*crosses*). Over half of the radio galaxies have cores that are not detected with VLBI, leading to upper limits on F_c. The pattern of Figure 1, that low F_c sources have low polarization, and high F_c sources have high polarization, is reinforced with this larger sample. The probability that high polarization ($p > 3\%$) and radio compactness $F_c > 0.1$ are not related is 0.043 for the galaxies in the VLBI sample alone. This drops to

NOTES TO TABLE 1

COLS. (1) and (2).—IAU name and other names.

COL. (4).—5 GHz flux density, from Pearson & Readhead 1988.

COLS. (5) and (6).—V magnitude and classification of optical counterpart. Compact radio sources are highly variable, and the flux densities and magnitudes are not simultaneous with the polarization measurements.

COLS. (8)–(10).—Degree of polarization and error, polarization position angle and error (in degrees), and date of observation. If more than one measurement was made, the *first* is listed.

COLS. (11)–(13).—Highest published degree of polarization, total number of observations published, including this work, and reference, as follows: (1) this paper; (2) Biermann et al. 1981; (3) Maza 1979; (4) Kühr & Schmidt 1989; (5) Angel & Stockman 1980; (6) Moore & Stockman 1984; (7) Smith et al. 1987; (8) Antonucci 1984; (9) Wills et al. 1980; (10) Miller 1975; (11) Stockman, Moore, & Angel 1984.

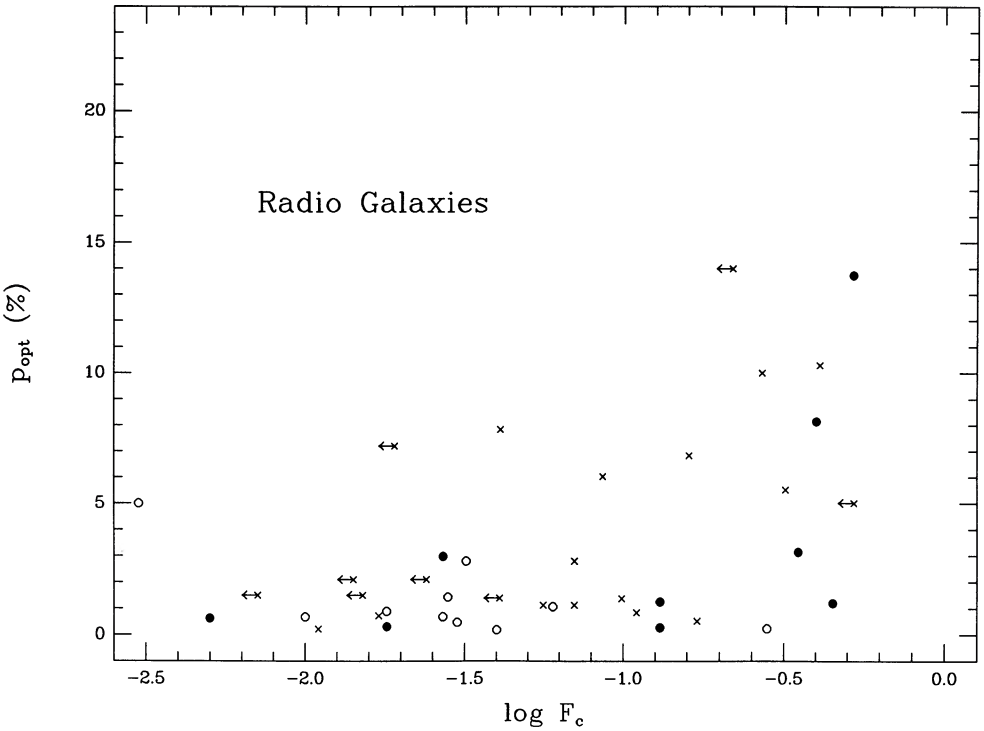

FIG. 2.—First measured value of optical polarization vs. the fraction of the radio flux density in a VLBI core for objects identified with galaxies. Circles are the same as in Fig. 1, crosses are galaxies and BL Lac objects from the literature.

0.029 if the two radio galaxies with high polarization and high upper limits on F_c in fact have $F_c < 0.1$. If the other galaxies and BL Lac objects from the literature are added in (crosses in Fig. 2), the probability falls to 0.0022. Note that the larger scatter of the crosses in Fig. 2 is due to the fact that F_c is estimated from VLBI visibilities at 2.29 GHz (Preston et al. 1985). Even so, the additional data points strengthen the correlation between F_c and p. The trend is not caused by a dependence of either quantity on luminosity. This is confirmed by Wehrle et al. (1984), who found that the fraction of B2 radio galaxies with detected cores was the same at all redshifts.

3.2. *Polarization Mechanism*

The interpretation of Figure 2 is complicated by the fact that a number of mechanisms can contribute to the observed polarization. First, we must account for interstellar polarization from our own Galaxy. Impey & Tapia (1988) gave measurements of interstellar polarization as a function of Galactic latitude in the fields of 105 extragalactic radio sources. Interstellar polarization was less than 0.5% in $\frac{2}{3}$ of the measurements, less than 1% in $\frac{4}{5}$ of the measurements, and never above 3%. Therefore in the division of sources into groups above and below 3%, polarization imprinted by aligned dust grains in the Galaxy can be neglected. Polarization from the interstellar medium of the radio galaxy itself is difficult to quantify. However, it is clear that polarization can be caused by scattering from dust and hot electrons near the nucleus of the active galaxy. Rudy et al. (1983) and Antonucci (1984) have published polarimetry of radio galaxies, and they conclude that it is difficult to disentangle thermal and nonthermal origins for the polarization. Rudy et al. (1983) find that the Stokes parameters do not generally vary, and that polarization is correlated with the decrement of the broad components of the Balmer lines. Spectropolarimetry by Antonucci (1984) also points to a scattering origin of the polarization in some cases. However, a small number of radio galaxies show variable polarization on time scales too small to be due to dust or electron scattering. This result is controversial, since the polarization level is low and small apertures are required to isolate the polarized nucleus from the surrounding (unpolarized) galaxy. If variability is confirmed, then weak synchrotron components must exist in the galactic nuclei.

The difference between quasars that are known to be synchrotron emitters and radio galaxies is illustrated in Figure 3, which attempts to show the variability of these radio sources in an unbiased way. Figure 3 is a plot of all radio sources with only two published polarization measures or sources where the first two measures could be unambiguously selected. Some well-studied objects are excluded, because the initial observations indicating high polarization were not published. Observations made earlier than 1967 are also excluded, because the polarization errors are generally above 1%. Observations made during the same lunation were not considered to be independent; the median time difference between the two measurements is 1 year. The final set of radio sources with two polarization measures consists of 21 radio galaxies and 47 quasars. Impey & Tapia (1990) presented a similar figure for 40 quasars, and we have added seven more from the VLBI sample. Only three of the 21 radio galaxies (*filled circles*) have $p_1 \neq p_2$ at the 2 σ level. Since systematic errors may easily affect any estimate of polarization variability, the evidence for synchrotron polarization is weak. The two highly polarized radio galaxies in Figure 3 with $p_1 \approx p_2$ are 3C 109 and 3C 234. The polarization in both these sources is likely to be due to scattering (Antonucci 1984; Rudy et al. 1983). This is in sharp contrast to the many quasars, where the polarization is strong and variable. Note that low-polarization quasars ($p < 3\%$) show no more evidence for variability than radio galaxies.

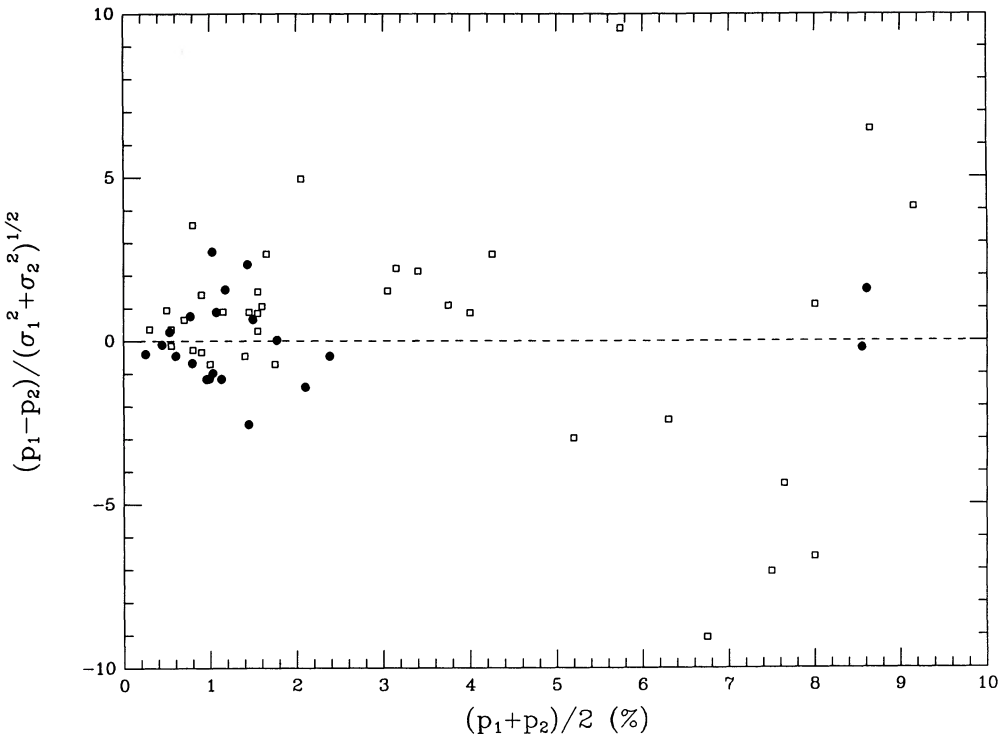

FIG. 3.—Polarization variability vs. polarization for objects in the sample or the literature for which the first and second measurements could be unambiguously determined (see text). Filled circles and open squares are galaxies and quasars, respectively.

We can draw two conclusions from the level and variability of polarization in Figure 3. First, interstellar polarization in our own Galaxy is a minor component in the low levels of radio galaxy polarization. Most radio galaxies have 1%–2% of intrinsic polarization. Second, $p > 3\%$ is seen rarely in radio galaxies and usually with a variability that indicates a synchrotron origin. The few cases of high-scattering polarization are not variable, and they are also identifiable by their radio properties. In Figure 1, the two galaxies with $p > 3\%$ and the lowest values of F_c are 3C 109 and 3C 234.

3.3. *Detecting Optically Polarized Cores of Low Luminosity*

We can test the hypothesis that *all* radio galaxies contain optically polarized cores, with strength proportional to the strength of the core radio emission, by modeling the optical emission as an unresolved polarized component at the center of an elliptical galaxy. The visibility of such a component galaxy on the continuum strength and polarization of the core, the luminosity of the host galaxy, the redshift, and the size of the aperture used for the polarimetry. Two quantities are calculated. The first is the stellar luminosity contained in an aperture of a given angular size as a function of redshift. The 1.″3 aperture used in these observations subtends $\sim 19z$ kpc at low redshift ($H_0 = 100$ km s^{-1} Mpc^{-1}). The second is the nonthermal optical luminosity one would expect from an unresolved core under the assumption that the optical and core radio flux densities are directly proportional.

Schneider, Gunn, & Hoessel (1983) have measured the structural parameters of a large number of ellipticals in clusters, and find that the galaxies are well fitted by a de Vaucouleurs model. In particular, first-ranked cluster galaxies have mean effective radii, $R_e = 34$ kpc, and a structural parameter, $\kappa = (d \ln L/d \ln r)_{r=19\,\mathrm{kpc}} = 0.70$. We calculate the fraction of total galaxy flux in a 1.″3 aperture for three absolute magnitudes, $M_V = -22$, -23, and -24. These values encompass 90% of powerful radio galaxies and known BL Lac objects (Ulrich 1989). The structural parameters of radio galaxies differ slightly from those of cluster galaxies of the same absolute magnitude (Lilly, McLean, & Longair 1984), but this has only a minimal effect on the calculation. We adopt values of $\kappa = 0.25$ ($M_V = -22$), $\kappa = 0.45$ ($M_V = -23$), and $\kappa = 0.80$ ($M_V = -24$). Also, the small aperture measurements sample regions in low-redshift galaxies that depart from a de Vaucouleurs law. Within the core radii of 0.5 kpc ($M_V = -22$), 1 kpc ($M_V = -23$), and 2 kpc ($M_V = -24$), the surface brightness is assumed to be constant (Kormendy 1986).

To calculate the luminosity of a nonthermal, unresolved core, we assume that the radio-optical spectral index for this core is $\alpha_{ro} = -0.73$, the average found by Impey & Neugebauer (1988) for a sample of 105 blazars. In general in this paper, we define spectral indices by the relation $S \propto \nu^{\alpha}$. This corresponds to $(S_r/S_0)_{\mathrm{core}} = 4750$, where S_r is the flux density determined by VLBI measurements. Since the optical core will be unresolved, no seeing correction has been made.

Figure 4 shows the estimated optical core luminosity versus redshift for the galaxies in the sample. The lines show the model stellar luminosity in a fixed aperture for the three values of the galaxy absolute magnitude. Galaxies with $p > 3\%$ are shown as open circles, while galaxies with $p < 3\%$ are shown as filled circles. This assumes that the nonthermal core has $p = 10\%$. Upper limits on F_c have been translated into upper limits on optical L_{core}. M82 lies far off to the left on Figure 4 at low redshift, with low polarization and a limit on L_{core} that places it below the three galaxy curves. The data in Figure 4 clearly support the idea that polarized optical luminosity is proportional to radio core luminosity. Galaxies situated above

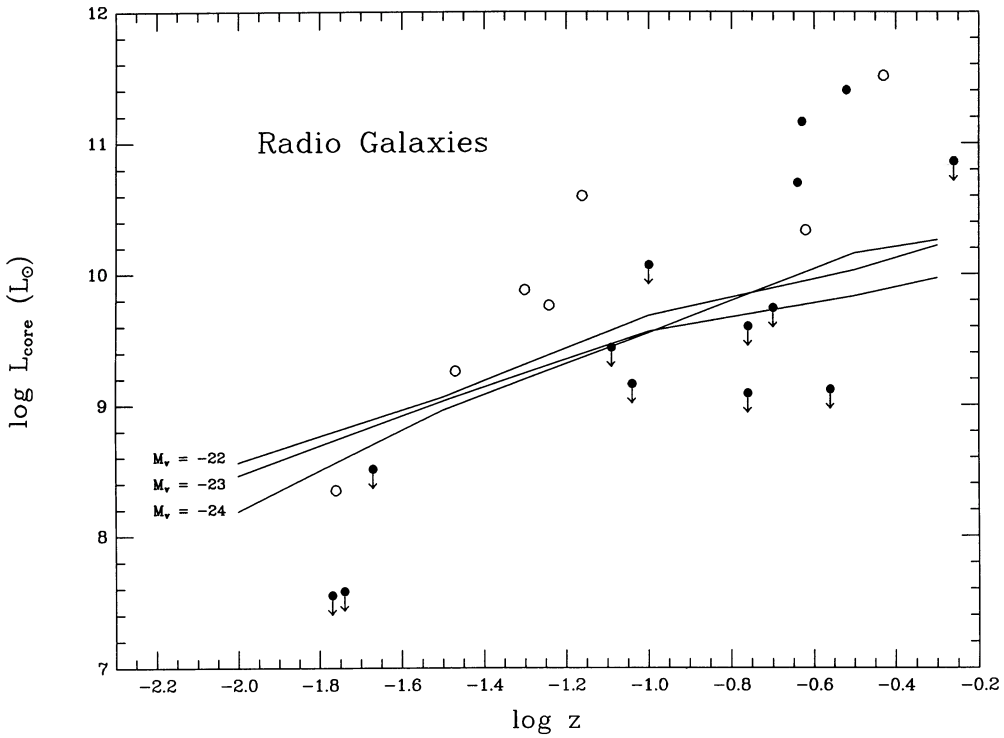

FIG. 4.—Estimated optical core luminosity in solar units plotted against redshift for radio galaxies measured in a 1".3 aperture. The solid lines represent the enclosed starlight from an elliptical galaxy ($H_0 = 100$ km s^{-1} Mpc^{-1}) and are not parallel because of the way that the radial profiles change with M_V (see text). Optical core luminosity is assumed to be proportional to radio core luminosity with a proportionality given by a typical blazar (see text). Galaxies plotted as open circles have $p > 3\%$, galaxies plotted as filled circles have $p < 3\%$.

the three curves have nonthermal optical cores that outshine the starlight. Six out of the seven objects in the sample that have been called "BL Lac objects" are in this region. Conversely, 10 out of the 11 galaxies below the curves have low polarization. In this region, nonthermal polarization is diluted to low levels by the excess of starlight. The exact proportion of polarized cores expected as a function of L_{core} depends on the range of synchrotron polarizations, which is not well determined. However, the separation of high- and low-polarization sources by the model curves is significant at the 98% level. This improves to 99.6% if the two radio galaxies with upper limits above the curve actually lie below the curves. Polarized cores are seen covering a luminosity range of more than 1000. The detectability of such cores appears to depend primarily on F_c, the compactness of the radio emission.

4. POLARIZATION IN QUASARS

4.1. *Polarization and Radio Compactness*

Figure 5 shows the first recorded measure of optical polarization plotted against the fraction of the 5 GHz flux density emerging from a milliarcsecond core, F_c. The radio compactness parameter is listed for the entire VLBI sample in Table 2. Filled squares show the 27 quasars with polarimetry in the complete 5 GHz VLBI sample; an additional two sources plotted with open squares have upper limits on F_c. Crosses represent similar data from the study of a complete sample of 2 and 1.5 Jy quasars by Impey & Tapia (1990), omitting the sources in common with the VLBI sample. We note that for the Impey & Tapia quasars, F_c is estimated from the VLBI visibilities measured at 2.29 GHz. However, in most cases the compactness values measured at the two frequencies agree to within a factor of 2, based on the sources in common between the two samples. Echoing the result for radio galaxies, Figure 5 shows that low F_c sources have low polarization, and high F_c sources have high polarization. The probability that radio compactness and polarization are not correlated is 0.074 for the VLBI sample, falling to 0.0053 if the 2 and 1.5 Jy quasars are added. Since the 2 and 1.5 Jy quasars have a crude measure of compactness, scatter in this quantity causes them to fill in a larger region of the F_c–p plane than the VLBI sample. This is also the reason that Impey & Tapia (1990) reached a different conclusion on radio and optical beaming than is found in this paper. Once again, this trend is not caused by a dependence of either quantity on luminosity or redshift. The fraction of quasars with high polarization rises from $\sim$20% for $F_c < 0.1$ to 45% for $F_c > 0.1$

4.2. *Duty Cycle of Polarization*

Synchrotron polarization in active galactic nuclei is characterized by an extreme degree of variability. Significant changes in the degree of polarization can be seen on time scales as short as one day (Angel et al. 1978). We have made an arbitrary separation between high and low polarization at 3%, based primarily on the fact that quiescent components such as interstellar polarization are negligible at that level. However, some of the sources with a maximum polarization above 3% will spend some of the time with $p < 3\%$. Maximum polarization is correlated with the number of observations in Table 1, for both quasars and radio galaxies. This reflects the fact that sources with extreme and unusual characteristics are the targets of campaigns of polarimetric monitoring. Because of this, we will use the first measured polarization value rather than p_{max} in our comparisons of polarization with other properties. The duty cycle of high- and low-polarization states can only be

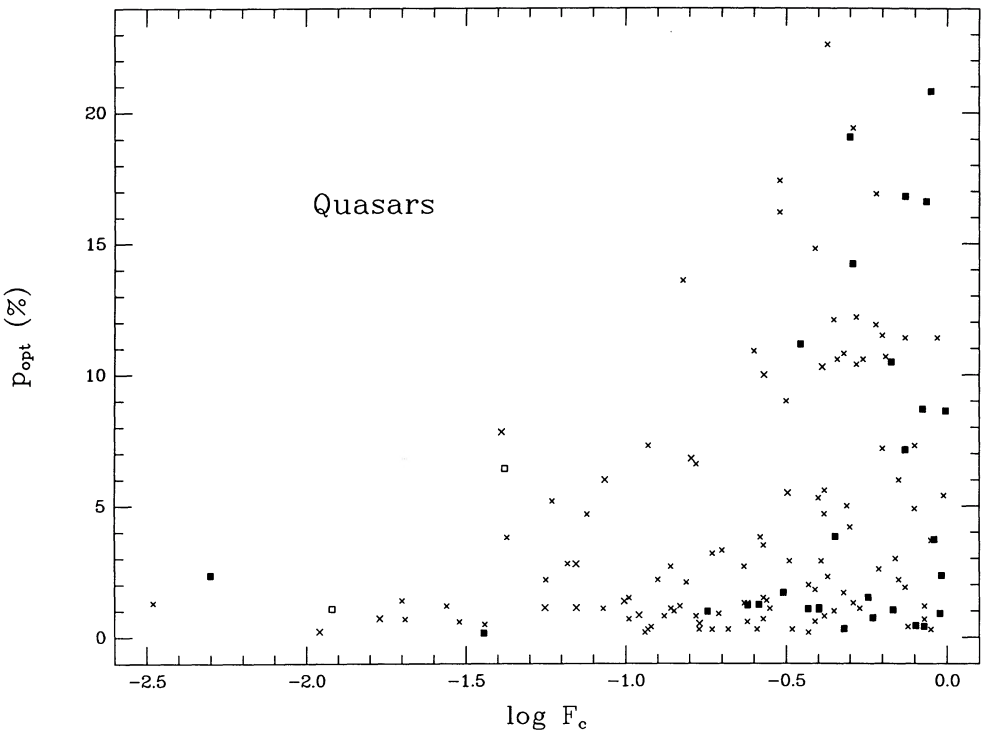

FIG. 5.—First measured value of optical polarization plotted against the fraction of the radio flux density in a VLBI core. Filled squares are quasars in the 5 GHz VLBI sample, open squares represent quasars with upper limits on F_c. Crosses are quasars from the complete sample studied by Impey & Tapia (1990).

estimated for a handful of blazars, and they are not likely to be a typical subset. Fugmann & Meisenheimer (1988), Impey & Tapia (1990), and Kühr & Schmidt (1989) have considered the duty cycle of polarization in flat spectrum quasars, and all estimate that $\frac{2}{3}$ have polarizations above 3% some of the time.

The histograms of first epoch polarizations for the quasars and radio galaxies in the VLBI sample are shown in Figure 6. Among the quasars, 13 out of 28 (46% $\pm$ 12%) have $p_1 > 3\%$. Therefore, single-pass polarimetry will reveal high polarization in nearly half of the quasars in a complete high-frequency radio sample, and the fraction is a function of radio compactness (Fig. 5). The median time interval between p_1 and p_2 is 1 yr; 23 out of 47 (49% $\pm$ 10%) have $p_1 > 3\%$ and 26 out of 47 (55% $\pm$ 11%) have $p_2 > 3\%$. After two epochs of observation, the *minimum* percentage of quasars with $p_{max} > 3\%$ is 60%. We cannot exclude the possibility that *all* quasars with compact radio emission have $p_{max} > 3\%$, at least some of the time. It is also possible that the trend of increasing numbers of polarized sources with radio compactness reflects a difference in the duty cycle of polarization. If the most compact quasars spent more of their time in a highly polarized state, then the result from Figure 5 could be explained.

4.3. *Blazar Components Plus Quiescent Components*

High and variable optical polarization is most likely to be seen in the most compact radio sources. We can demonstrate that this applies to optical flux variability also. Figure 7 shows the peak-to-peak amplitude of flux variability for 103 quasars from the 19 yr monitoring programs of Pica et al. (1988) and Webb et al. (1988). Filled squares represent sources where the confidence level of detecting real variations is greater than 99.5%. Only four of these quasars are in the VLBI sample, the core fraction F_c has been estimated for the rest using the visibility parameters of Preston et al. (1985). Impey & Tapia (1990)

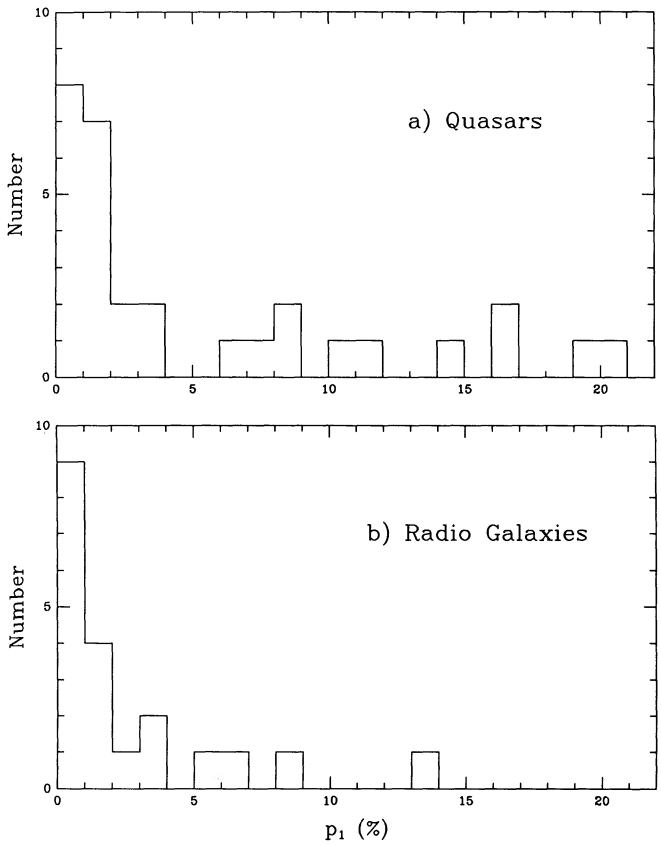

FIG. 6.—Histogram of first measured polarization measurement for (*a*) quasars and (*b*) radio galaxies.

TABLE 2

OPTICAL AND RADIO PROPERTIES

Source (1)	α_r (2)	F_c (3)	θ_{VLB} (4)	p_r (5)	θ_r (6)	$\Delta\theta_1$ (7)	$\Delta\theta_2$ (8)	v/c (9)	L/C (10)	W_{eq} (11)	L_{320} (12)	L_5^{core} (13)
0016+731	+0.16	0.95	156	...	...	48	...	...	0.60	51	26.08	26.4
0040+517	−0.72	<0.003	...	4.1	90	...	...	...	2.78	51	25.95	...
0108+388	+0.49	0.75*	59	...	...	...	...	...	...	...	...	...
0133+476	+0.62	0.89	137	4.5	86	70	19	<1.3	1.31	8	25.90	25.9
0153+744	−0.32	0.40*	157	...	...	51	...	...	2.59	87	26.61	...
0210+860	−1.2	<0.007	...	7.6	41	...	...	...	4.20	70	25.80	...
0212+735	−0.12	0.59	101	...	...	12	...	3.9	0.31	95	26.73	26.5
0220+427	−0.87	<0.06	...	...	...	...	...	...	0.50	5	24.02	...
0314+416	−0.54	<0.01	...	7.8	106	...	3	...	...	...	23.82	...
0316+413	−0.51	0.005*	35*	1.3	50	79	64	0.2	6.61	502	23.97	...
0404+768	−0.58	0.031*	48*	...	...	...	...	...	...	...	...	...
0454+844	+0.38	0.51	141	...	...	51	...	...	0.0	...	...	...
0538+498	−0.76	0.005*	53*	3.1	48	64	59	...	3.87	44	27.11	...
0605+480	−0.89	<0.001	...	4.1	48	...	...	...	10.06	67	25.95	...
0710+439	−0.22	0.35*	0	...	...	...	...	<0.7	2.86	17	25.35	25.4
0711+356	−0.31	0.24	158	1.1	148	51	61	...	1.31	44	25.90	25.5
0723+679	−0.33	0.31	92*	1.2	123	90	59	4.8	...	...	26.53	...
0804+499	+0.49	0.99	140	0.8	45	39	46	...	...	...	26.07	26.2
0809+483	−0.88	<0.012	...	4.6	172	...	17	...	5.46	100	27.56	...
0814+425	+0.68	0.84	149	5.5	148	13	14	...	0.0	...	...	...
0831+557	−0.46	0.027*	43*	0.6	162	40	21	...	...	...	25.63	...
0836+710	−0.33	0.40	34	...	...	68	...	6.3	0.34	22	27.13	26.3
0850+581	+0.78	0.85	156	...	...	8	...	3.9	0.62	46	26.18	26.0
0859+470	−0.09	0.68	0	4.1	67	20	47	...	1.08	82	26.66	26.1
0906+430	−0.46	0.45	155	1.4	22	78	31	2.4	0.96	3	26.85	25.4
0917+458	−1.4	<0.018	...	4.9	131	...	...	...	2.09	183	25.87	...
0923+392	+1.0	0.80*	97	0.9	81	19	35	3.5	1.42	81	26.26	...
0945+408	+0.08	0.48	127	6.5	7	...	...	...	0.66	57	26.80	...
0951+699	−0.66	<0.018*	60*	0.9	48	21	9	...	...	...	...	...
0954+556	−0.23	<0.042*	...	4.9	3	...	2	...	0.27	11	26.52	...
0954+658	+0.30	0.50*	126*	...	...	44	...	...	0.0	...	25.02	...
1003+351	−0.69	<0.28	110*	1.2	174	...	...	...	...	...	24.89	...
1031+567	−0.30	0.13*	...	0.1	...	...	...	...	...	...	25.62	...
1157+732	−0.72	<0.015	...	2.9	131	...	...	...	...	...	27.19	...
1254+476	−1.0	<0.007	...	9.6	91	...	...	...	12.20	265	27.22	...
1358+624	−0.67	0.06*	125*	0.1	...	...	...	...	2.65	5	25.98	...
1409+524	−0.95	<0.009	...	2.8	122	...	...	...	3.39	72	27.04	...
1458+718	−0.66	0.18	162*	3.0	33	55	74	...	0.22	10	27.12	25.5
1609+660	−0.78	<0.032	...	4.3	141	...	...	...	34.56	44	26.76	...
1624+416	−0.29	0.35	59	0.7	...	...	...	...	...	...	27.04	26.1
1633+382	+0.77	0.37	115	1.3	173	1	59	...	1.88	92	26.54	26.1
1634+628	−0.95	<0.03*	...	2.0	27	...	...	...	15.63	358	26.97	...
1637+574	+0.55	0.96	7*	...	...	17	...	...	0.60	79	25.18	25.8
1641+399	−0.53	0.35	68*	4.0	40	15	13	9.5	0.96	34	26.47	25.8
1642+690	−0.26	0.86	15	5.0	154	7	34	7.9	0.48	12	25.92	25.8
1652+398	−0.02	0.35	133	4.2	156	8	31	...	0.13	7	23.26	22.6
1739+522	+0.07	0.91	3	2.3	86	11	86	...	0.14	11	26.06	26.0
1749+701	−0.33	0.67	116	4.0	120	13	9	>2.2	0.0	...	...	...
1803+784	+0.26	0.74	88	5.8	80	83	89	<0.6	0.20	11	25.66	25.8
1807+698	−0.35	0.40	83	5.0	175	23	69	...	0.11	7	23.96	23.3
1823+568	+0.17	0.74	17	2.3	49	3	29	...	0.12	10	25.98	25.5
1828+487	−0.53	0.036*	123*	0.4	...	19	...	...	4.25	71	27.34	...
1842+455	−0.93	<0.03	...	1.7	146	...	5	...	0.54	20	25.11	...
1845+797	−0.69	0.13	143	4.9	16	7	60	1.9	10.31	674	24.98	22.9
1928+738	−0.01	0.26	166	...	...	23	...	7.0	5.78	483	25.28	25.2
1939+605	−0.99	<0.028	...	2.5	174	...	...	...	0.93	61	25.80	...
1954+513	−0.14	0.57	8	0.9	67	24	83	...	0.35	6	26.68	25.9
2021+614	+0.10	0.13*	32	0.2	...	...	...	<0.6	1.34	72	24.86	...
2153+377	−1.2	<0.007	...	3.1	173	...	...	...	0.72	26	26.41	...
2200+420	−0.15	0.52	3	2.7	0	15	18	2.4	0.0	...	23.95	23.7
2229+391	−0.94	<0.027	...	7.1	68	...	57	...	0.21	11	23.39	...
2243+394	−0.96	<0.04	...	9.6	126	...	41	...	1.25	42	25.37	...
2342+821	−0.92	...	...	...	...	...	...	...	...	...	26.93	...
2351+456	−0.07	0.29	107	...	...	...	...	...	...	...	26.79	25.8
2352+495	−0.34	0.45	178	1.6	174	...	...	...	1.21	44	25.12	24.5

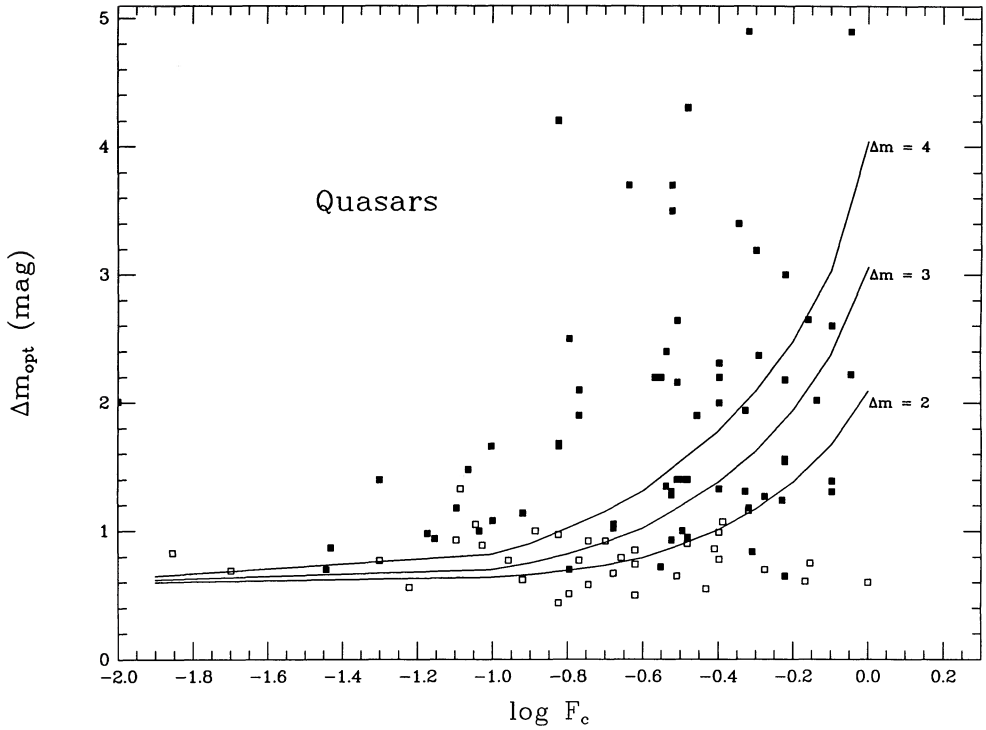

FIG. 7.—Peak-to-peak amplitude of optical flux variability plotted against the fraction of radio flux density in a VLBI core, estimated for objects not in the VLBI sample from the visibility parameters given by Preston et al. (1985). Variability information is from Pica et al. (1988) and Webb et al. (1988). Filled squares are those quasars where the confidence level on the detection of variability is above 99.5%. Curves are plotted for a model where F_c is proportional to the fraction of optical flux density in a variable, polarized component (see § 7).

have shown that for 140 core-dominated quasars, the VLBI visibility (i.e., correlated flux density for some specified fringe spacing) is a good estimator of the fractional flux density in the core. The variability sample of Pica et al. (1988) and Webb et al. (1988) is not complete, but it is not biased with regard to F_c. Figure 7 can be compared with Figure 5. A similar monotonic rise in both p and Δm with F_c is seen. Including the 2 and 1.5 Jy quasars, the fraction with $p_{opt} > 3\%$ rises from 20% at $F_c < 0.1$ to 45% at $0.3 < F_c < 1.0$. Making a simple correction for the duty cycle of high- and low-polarization states, these fractions become 26% and 59%. Similarly, the fraction of quasars with $\Delta m_{opt} > 1.2$ (twice the noise level) rises from 29% at $F_c < 0.1$ to 66% at $0.3 < F_c < 1.0$.

The best measure of the dependence of p and Δm on F_c uses only the VLBI sample, since core fractions are determined reliably from component-fitting of the VLBI maps. Also, it may not be appropriate to compare polarization with a global measure of peak-to-peak flux variability. The tabulations of Pica et al. (1988) and Webb et al. (1988) quote Δm on time scales of years. However, the time scale corresponding to the polarization variability is weeks (Smith et al. 1985; Sitko, Schmidt, & Stein 1985). Data from the monitoring programs can be used to extract peak-to-peak flux variability amplitudes on 1 month time scales for 70 radio sources. The results are that only 8% (1/13) of the sources with $F_c < 0.1$ have $\Delta m > 1$ mag, whereas 56% (32/57) of the sources with $F_c > 0.1$ have $\Delta m > 1$ mag. In the VLBI sample, we find that 7% (1/15) of the sources with $F_c < 0.1$ have $p > 3\%$, whereas 52% (17/33) of the sources with $F_c > 0.1$ have $p > 3\%$. The behaviors of polarization and flux variability as a function of radio compactness are

NOTES TO TABLE 2

COL. (2).—Spectral index between 2.6 and 5 GHz, where $S \propto \nu^{\alpha}$.

COL. (3).—Fraction of radio flux density in an unresolved VLBI core, as given by Pearson & Readhead 1988 for 48 sources. For the 16 sources marked with an asterisk F_c has been estimated from the 2.29 GHz visibilities measured by Preston et al. 1985.

COL. (4).—Position angle of the VLBI core, from Pearson & Readhead 1988, or if marked with an asterisk, Rusk 1988.

COLS. (5) and (6).—Maximum 5 GHz radio polarization and position angle. The principal source of radio polarimetry is the compilation of Rusk 1988, with some data from Tabara & Inoue 1980.

COL. (7).—Position angle difference between the VLBI structure axis and the radio polarization.

COL. (8).—Position angle difference between the VLBI structure axis and the optical polarization (from Table 1).

COL. (9).—Apparent proper motion of VLBI components in units of the speed of light.

COLS. (10) and (11).—Line to continuum ratio and the equivalent width of the strongest permitted line from measurements of the optical spectrum.

COL. (12).—Logarithm of the total luminosity per steradian at a rest frequency of 320 MHz ($H_0 = 100$ km s^{-1} Mpc^{-1}, $q_0 = 0.5$), in W Hz^{-1} sr^{-1}. The observed flux density at the equivalent redshifted frequency was estimated from weighted spline fits to published flux density measurements by T. Herbig (private communication). For all but the most extreme core-dominated sources, beamed emission is unimportant at this frequency; even in extreme cases beamed emission is likely to contribute only about half the total observed flux density. Thus this column gives a reasonable approximation to the bolometric radio luminosity of the source. Nevertheless, we list luminosity per steradian to emphasize the point that bolometrically insignificant emission can dominate a source.

COL. (13).—Core luminosity per steradian at 5 GHz observed frequency ($H_0 = 100$, $q_0 = 0.5$), in W Hz^{-1} sr^{-1}. Core flux densities are from Pearson & Readhead 1988.

identical. In both cases, evidence for optical synchrotron emission increases dramatically when the radio source is sufficiently compact.

This connection between high polarization and large amplitude flux variability, first noted by Moore & Stockman (1984), implies that the variable flux component in quasars carries the high polarization. This leads to a picture in which the optical flux density of quasars consists of a relatively steady unpolarized component, and a highly variable and highly polarized component, i.e., a blazar. Although one component will generally dominate, the two contributions can be separated out in some radio sources (Impey, Malkan, & Tapia 1989). The detection of flux variability or high polarization in a quasar depends on the ratio of these two components.

5. RADIO AND OPTICAL PROPERTIES

Various radio and optical properties of the VLBI sample are summarized in Table 2.

5.1. *Distinction between Radio Galaxies and Quasars*

The 65 optical counterparts of the VLBI sample include 29 "galaxies" and 36 "quasi-stellar objects," classified according to their appearance on sky survey or CCD images, typically. Clearly, the distinction between radio galaxy and quasars depends on (1) the quality of the optical photograph or CCD image, (2) the distance of the source, (3) the luminosity of the host galaxy, and (4) the contrast between the stellar and nonstellar continua. Figure 8 shows F_c plotted against redshift for the quasars (*squares*) and radio galaxies (*circles*). Five sources do not have redshifts. Over half of the radio galaxies and four of the quasars have undetected VLBI cores, hence upper limits on F_c (Pearson & Readhead 1988). The range in F_c is at least a factor of 300, limited only by the sensitivity of VLBI experiments.

There are well known distinctions between radio galaxies and quasars. On average, quasars have stronger cores, more one-sided jets, and smaller linear dimensions than radio galaxies (Owen 1986; Miley 1980). Hutchings (1987) has found significant differences between radio galaxies and quasar host galaxies, using samples that are matched in radio luminosity and spectral index. Since quasars have stronger cores than radio galaxies, and cores typically have flatter spectra than extended emission, a large fraction of sources selected at a high radio frequency such as 5 GHz will be quasars.

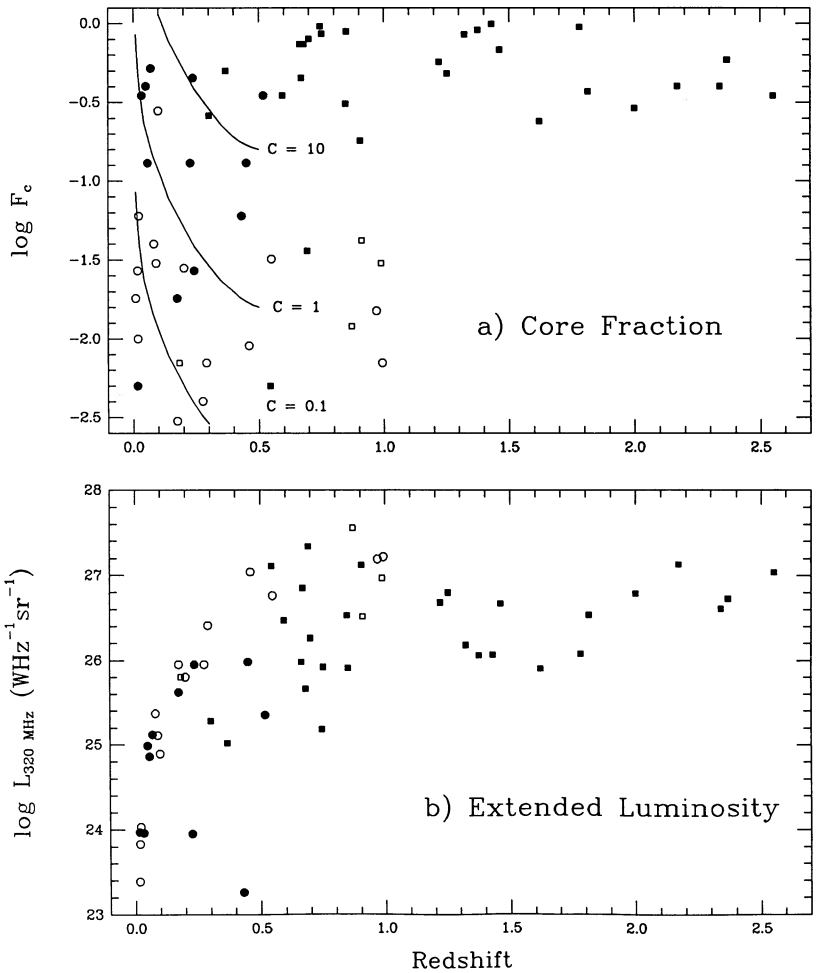

FIG. 8.—(*a*) Radio compactness on VLBI scales vs. redshift for quasars (*squares*) and radio galaxies (*circles*) in the VLBI sample. Open symbols are used for upper limits on F_c. Models are shown for three values of the ratio of nonthermal to stellar optical continuum (C). The calculation of C assumes a host galaxy with $M_V = -23$ and that the nonthermal optical flux is proportional to the core radio flux (see text for details). (*b*) Estimated luminosity at a rest frequency of 320 MHz (see notes to Table 2) vs. redshift. Even the most highly Doppler boosted components are unlikely to outshine the extended structure at this frequency due to self-absorption, so that L_{320} approximates the isotropic luminosity of the source.

The sources in Figure 8*a* are clearly segregated; quasars are more compact and have higher redshifts than radio galaxies. The absence of sources in the bottom right quadrant of Figure 8*a* is at least partly due to selection effects. Extended sources typically have a steep radio spectrum ($S \propto \nu^{-0.7}$). The higher the redshift, the higher the rest frequency at which the source is observed, and the weaker the extended sources will be relative to their flat-spectrum, compact counterparts. Moreover, in many, if not all, of the compact objects Doppler boosting exaggerates the apparent core luminosity at high frequencies. This can be seen in Figure 8*b*, which shows luminosity at a *rest* frequency of 320 MHz versus redshift. At 320 MHz, a frequency which is unaffected by beaming, the core-dominated sources are less luminous than the extended sources at a given redshift.

Figure 8*a* also includes tracks to show the detectability of a nonthermal optical component, on the assumption that it scales with core radio flux density (see Fig. 4 for support of this assumption). Three values of the contrast C are shown, where C is defined as the ratio of nonthermal optical to galaxy flux. We have used a 1".3 aperture and a galaxy with $M_V = -23$ for this calculation. For all but two of the quasars, but only half of the galaxies, nonthermal optical light is expected to dominate starlight from the host galaxy. From § 2, similar fractions of quasars and radio galaxies with $F_c > 0.1$ have $p > 3\%$. No conclusion can be drawn for $F_c < 0.1$, due to the smaller number of sources with polarimetry and the heavy dilution by starlight in the radio galaxies. Radio galaxies and quasars are similar in that the nonthermal optical component in each population appears to scale with the core radio flux density.

5.2. *Emission-Line Strength and Optical Polarization*

One of the distinctive features of the VLBI sample is the high-quality optical spectroscopy that is available. Spectra have been acquired using the double spectrograph on the Palomar 200 inch (5 m) telescope, with a typical wavelength coverage of 3800–9800 Å (Lawrence et al. 1986, 1987). Redshifts have proved elusive for five sources: two faint ($V \sim 22$ mag) galaxies and three continuum-dominated objects.

So far, we have considered only the morphological distinction between galaxies and quasars, which depends on data quality. Unfortunately, the spectroscopic distinction between strong and weak lined objects also depends on data quality, since the contrast of the observed emission lines depends on the (variable) strength of the continuum (e.g., Miller & French 1978; Lawrence et al. 1987; Lawrence 1990), the signal-to-noise ratio, the redshift of the source, and the wavelength coverage of the spectrum. Moreover, the detectability of the underlying galaxy depends on its luminosity. In the VLBI sample sources with emission lines of low equivalent width cover a wide range of low-frequency luminosities and an equally wide range of emission line luminosities (Lawrence 1990). Although it seems that every radio source with emission lines of low equivalent width is, sooner or later, called a "BL Lac object," we will use the term to refer only to the "classical" BL Lac objects found in low-redshift galaxies, which have both low radio luminosity and low emission-line luminosity. Since three of the missing redshifts in the VLBI sample are for objects with strong nonthermal continua, we are unable to apply strict radio and emission-line luminosity criteria to the problem of classifying "BL Lac objects." We recognize that there may be sources at high redshift with high polarization and weak emission lines, and these sources may or may not be related to the prototype.

Emission-line properties are plotted against optical polarization for quasars and radio galaxies in Figure 9. Figure 9*a* shows line to continuum ratio (L/C), and Figure 9*b* shows the equivalent width of the strongest permitted line. The two quantities are listed in columns (10) and (11) of Table 2. These lines have velocity widths of thousands of kilometers per second; there are only a few narrow line quasars and narrow line radio galaxies in the VLBI sample. The correlation between weak emission lines and high polarization is very strong for the quasars. The confidence level is 99.9% or better for both L/C and EW. All of the seven quasars with $L/C < 0.2$ have $p > 3\%$, whereas only five out of 22 quasars with $L/C > 0.2$ have $p > 3\%$. The result is insensitive to the status of the four quasars in the VLBI sample without polarimetry. The correlation for radio galaxies is not as strong; however, two out of three galaxies with $L/C < 0.2$ have $p_{\max} > 3\%$, whereas none of the 11 galaxies with $L/C > 0.2$ has $p_{\max} > 3\%$. The statistical significance is supported by the survey of strong sources by Impey & Tapia (1990). Combining the samples, 22 out of 23 (96%) quasars with weak lines have high polarization, as opposed to 44 out of 133 (33%) of the quasars with strong lines.

Optical polarization is correlated both with weak emission lines and large core fractions of the radio source, so we would also expect emission-line strength to be anticorrelated with radio compactness. This is confirmed, both for quasars and radio galaxies. When upper limits on F_c are excluded, F_c and L/C are anticorrelated at the 99.9% significance level for quasars, and the 90% significance level for radio galaxies.

5.3. *Superluminal Motion and Optical Polarization*

The quality and time coverage of VLBI data has improved steadily over the last 10 years. In a recent count, 29 radio sources have shown apparent superluminal motion of the milliarcsecond components (Cohen 1989). This number will undoubtedly increase as surveys now underway continue. Apparent superluminal motion is common among core-dominated quasars. Witzel et al. (1988) counted eight candidates out of 12 in the 5 GHz MPIfR–NRAO survey of strong sources. Impey (1987) pointed out that 70% of the confirmed superluminal sources in 1987 had blazar properties at optical wavelengths. We can pursue this connection with the large and complete VLBI sample described in this paper. Thirteen sources in Table 2 have apparent superluminal motion, the motion is subluminal (but highly relativistic) in four other cases. High polarization is seen in nine out of 13 of the superluminal sources, and two of the remaining four have only had one polarization measurement. This fraction is consistent with the fact that sources with superluminal motion are among the most compact in the sample.

Two other trends are apparent in the 18 sources with estimates of v/c. First, and not surprisingly, the five galaxies have slower apparent component separations than the 13 quasars (significant at the 99% confidence level). Second, quasars with weak emission lines tend to have lower values of v/c. This effect has also been claimed for classical BL Lac objects, using inhomogeneous data sets, by Impey (1987), Cohen (1989) and Gabuzda, Wardle, & Roberts (1989). The significance is better than 95% using the Mann-Whitney and Kolmogorov-Smirnov tests, but becomes weaker if 0454+844 and

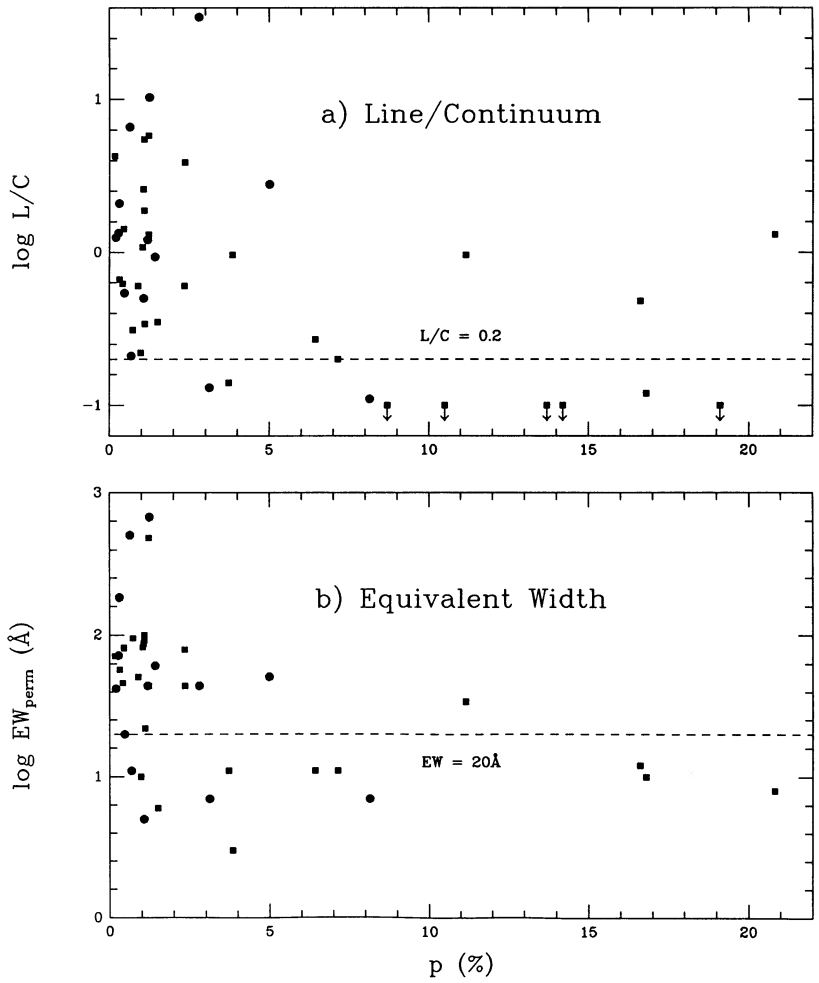

FIG. 9.—First measure of optical polarization plotted against (*a*) line to continuum ratio and (*b*) equivalent width of the strongest permitted emission line. Squares are used for quasars, circles for radio galaxies.

1749+701 have substantially faster separations than their minimum value of v/c would indicate (Witzel et al. 1988).

5.4. *Radio and Optical Polarization*

The connection between radio core emission and nonthermal optical emission is well established. However, it is useful to look for a geometric connection between the two wavelength regimes, to indicate whether or not the radio and optical emission come from the same volume. Compact radio sources often have one synchrotron component that dominates from 10^{11} to 10^{15} Hz (Landau et al. 1986; Impey & Neugebauer 1988). At a sufficiently high radio frequency, where the opacity is low, the signature of a single synchrotron component may show up in the polarization.

Figure 10*a* plots 2 cm polarization against maximum optical polarization for sources in the VLBI sample (*filled circles*) and for 49 other sources, mostly core-dominated quasars (*crosses*). The radio polarimetry is taken from Rusk (1988), based on a homogeneous set of VLA maps. Polarization at the two wavelengths is correlated at the 99% confidence level for the VLBI sample, and the confidence level is still above 95% when the Rusk sources are added. This correlation is completely absent at the longer wavelengths of 6, 18, and 22 cm. Figure 10*b* shows the difference between 2 cm and optical position angle as a function of optical polarization. The higher the optical polarization, the closer the alignment between radio and optical position angles. This result is significant at the 99% confidence level (99.9% for $p_{opt} > 3\%$). At longer wavelengths, this effect weakens, until at 22 cm, high optical polarization is associated with a *misalignment* between radio and optical position angles. The 2 cm and optical data were not obtained simultaneously, but any source variability will only *weaken* the trends seen in Figure 10. These results are consistent with a lower source opacity at 2 cm, such that optically thin synchrotron emission from a similarly aligned magnetic field is seen at 2 cm and at optical wavelengths. It is also possible that a single energy distribution of electrons gives both the radio and optical polarized emission.

5.5. *Position Angle Alignments*

A striking alignment has been observed between the position angle of compact radio source structure and the position angle of optical polarization (Rusk & Seaquist 1985; Impey 1987). A comprehensive study of position angle alignments at radio and optical wavelengths has been carried out by Rusk (1988). The position angle alignment implies a connection between the axis of radio jet collimation, and the orientation of the magnetic field imprinting the synchrotron polarization. The alignment is in the sense that the distribution of values of $|\theta_{VLBI} - \theta_{opt}|$ is peaked at values near zero. Since polarization position angle

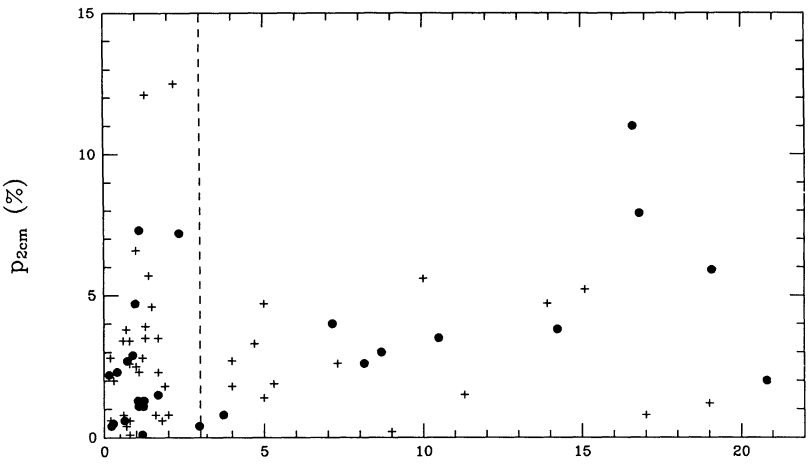

FIG. 10*a*

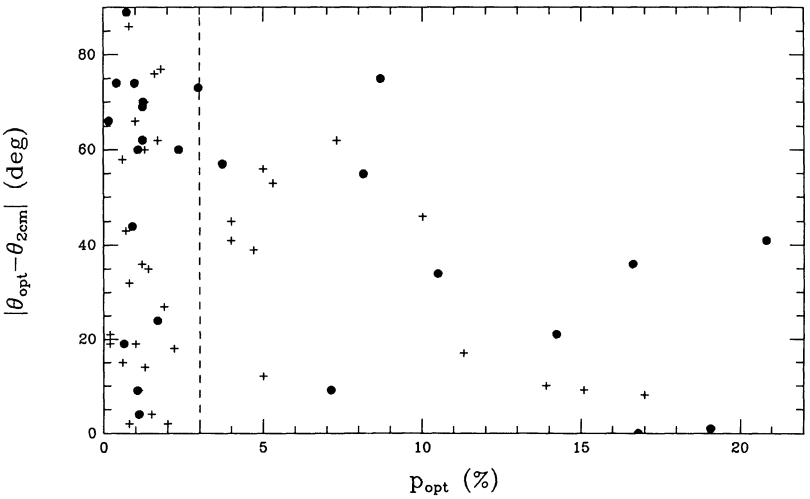

FIG. 10*b*

FIG. 10.—Maximum optical polarization vs. (*a*) 2 cm radio polarization and (*b*) position angle difference between radio and optical polarization. The radio polarimetry is from Rusk (1988), with filled circles for the VLBI sample, and crosses for other sources, mostly core-dominated quasars.

has a 180° ambiguity, the range of $|\theta_{VLBI} - \theta_{opt}|$ is 0°–90°. The definition of $|\theta_{VLBI} - \theta_{opt}|$ for a particular radio source is complicated for several reasons. Some blazars have polarization position angles that vary from 0° to 180°, while others have position angles that cluster in a small range. Impey (1987) considered a blazar to have a *preferred* polarization position angle if at least $\frac{2}{3}$ of the published measurements lie in a range of 40° or less. This criterion excludes some of the most well-known blazars and classical BL Lac objects. Conversely, if the polarization is low, the poor signal-to-noise ratio will give a large error in the position angle. The orientation of the VLBI structure axis can also depend on the frequency of the map. Some sources show significant curvature at milliarcsecond scales.

It is important to test for the position angle alignment in a large and homogeneous sample, since unknown selection effects may have influenced earlier studies. Thirty-five sources in the VLBI sample have both optical polarimetry and VLBI structure angles. Since so many of the sources have only one polarization measurement, we calculate $|\theta_{VLBI} - \theta_{opt}|$ using the first measured position angle (col. [9] in Table 1). In two cases, we used the second published measurement, where the first had too low a signal-to-noise ratio to determine a position angle. This circumvents the problem of the incomplete sampling of position angle variations. However, it means that the distribution of $|\theta_{VLBI} - \theta_{opt}|$ will be smeared out compared to the distribution formed using long-term averages of polarization position angle. We use VLBI structure angles measured at 5 GHz where possible, and estimate that the mean error in θ_{VLBI} is 6°–8°. The distributions of $|\theta_{VLBI} - \theta_{opt}|$ are plotted in Figure 11. The sample is divided by high and low polarization in Figures 11*a* and 11*b*, and by quasars and galaxies in Figures 11*c* and 11*d*.

The peak at $|\theta_{VLBI} - \theta_{opt}| \sim 0°$ for the whole sample is highly significant—the probability from a χ^2 test that it is uniformly distributed is only 0.0025. The deviation from a uniform distribution comes mainly from the highly polarized sources, where the probability of a uniform distribution is 0.0054, while the distribution of $|\theta_{VLBI} - \theta_{opt}|$ for low-polarization sources alone is not significantly different from a uniform distribution. We emphasize that rotation of the optical position angle, which is observed in many strong radio sources, can only act to *reduce* the deviation from a uniform distribution. The peak in Figure 11*a* is very narrow. The mean measurement error on θ_{opt} for highly polarized sources is only 2°, so the measurement error on $|\theta_{VLBI} - \theta_{opt}|$ is $\sim 7°$. The sharpness of the peak at 0° indicates that many blazars do *not* have a large range of polarization position angles. The mean measurement error on θ_{opt}

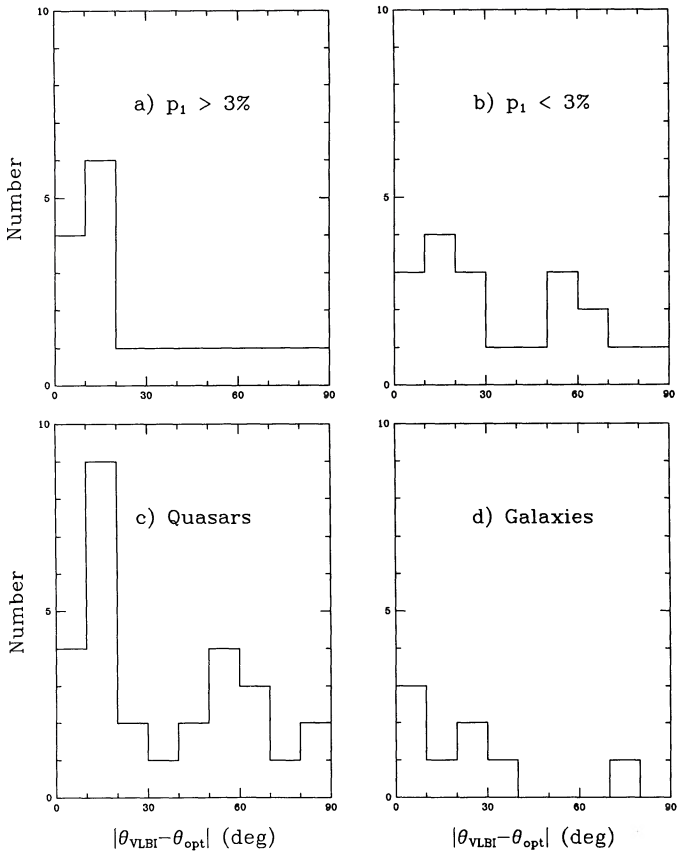

FIG. 11.—The difference between the position angle of the VLBI structure axis and the position angle of optical polarization for 35 sources, divided by (*a*) $p_1 > 3\%$, (*b*) $p_1 < 3\%$, (*c*) quasars, and (*d*) galaxies.

for low polarization sources is 11°, so the measurement error on $|\theta_{VLBI} - \theta_{opt}|$ is $\sim 13°$. Therefore, the more uniform distribution of Figure 11*b* is not due to observational error. We note that classical BL Lac objects show a position angle alignment; six out of 10 have $|\theta_{VLBI} - \theta_{opt}| < 20°$.

The interpretation of position angle alignments depends on the emission mechanism of the polarized radiation. Antonucci (1983, 1984) has studied polarization and arcsecond radio structure in low-luminosity active galactic nuclei. Radio structure and optical polarization are usually aligned for Seyfert 1 galaxies and radio galaxies, and orthogonal for Seyfert 2 galaxies (Alighieri et al. 1990; Jannuzi & Elston 1991). Scattering by dust or electrons is thought to produce the orthogonal polarization, and in some cases such as 3C 382 it may cause the aligned polarization as well (Antonucci 1984). Low-polarization quasars have position angles that align with both the large and small-scale radio structure (Stockman, Angel, & Miley 1979; Impey 1987; Rusk 1988). We find that low-polarization quasars do not show as strong an alignment around $|\theta_{VLBI} - \theta_{opt}| \sim 0°$ as the high-polarization quasars. Since the emission mechanism leading to the low polarization seen in most quasars is uncertain, we restrict our attention to the highly polarized synchrotron emitters.

The best insight into the alignment seen in Figure 11*a* comes from VLBI polarimetry. The first published results deal primarily with around a dozen highly polarized quasars and classical BL Lac objects (Wardle & Roberts 1988; Gabuzda et al. 1989; and references therein). The maps indicate that while core emission dominates the total intensity, most of the polarized intensity comes from the milliarcsecond jets. The percentage polarization of knots in the jets can be as high as 60%. Cores are typically a couple of percent polarized. The optical polarization of both highly polarized quasars and BL Lac objects indicates a projected magnetic field *perpendicular* to the VLBI jet axis (Impey 1987; Rusk 1988; this paper).

On VLBI scales, the magnetic field in BL Lac objects is perpendicular to the jet axis (Gabuzda et al. 1989), as it is at optical wavelengths. In 10 out of 11 BL Lac objects, the alignment is better than 25°. In contrast, the ***B*** vectors in the cores of these objects are parallel to the jet axis. On VLA scales the magnetic field is perpendicular (or bimodal) to the jet axis (Rusk 1988, 1990). For highly polarized quasars the situation on VLBI scales is uncertain, since only one has been published (Wardle et al. 1986), but on VLA scales the ***B*** vector is parallel to the jet axis. Suppose that in all highly polarized objects the direction of the magnetic field to the VLBI-scale structure is parallel in the core, perpendicular in the jet close to the core, and parallel in the jet further out. Then these alignments are consistent with a picture in which the dominant polarized optical emission comes from the inner part of the jet in all highly polarized objects, while the relative strengths of the core (stronger in quasars) and inner jets (stronger in BL Lac objects) determines what is seen in VLBI observations. One model explains these alignments as the result of strong shocks compressing a tangled magnetic field into a sheet perpendicular to the jet axis (Aller, Aller, & Hughes 1985; Aller, Hughes, & Aller 1987; Jones 1988; Cawthorne & Wardle 1988).

Finally, we point out another interesting relationship between optical polarization and radio structure in the VLBI sample. In addition to a structure axis on milliarcsecond scales, the orientation of the structure on arcsecond scales can be determined for many compact sources using VLA maps. In some cases this fails because the source is unresolved, or because the diffuse emission that surrounds the compact core in VLA maps is amorphous. However, 17 objects in the sample with polarimetry have a bend angle that can be defined between milliarcsecond and arcsecond scales. Rusk & Rusk (1986) have pointed out that the distribution of this bend angle can be used to constrain the Lorentz factor (or intrinsic misalignment parameter) in a relativistic beaming model. Five out of the eight objects in the VLBI sample with high polarization ($p_{max} > 3\%$) have a high degree of misalignment ($|\theta_{VLBI} - \theta_{arcsec}| > 70°$), whereas seven of the nine objects with low polarization have a small misalignment ($|\theta_{VLBI} - \theta_{arcsec}| < 25°$). There are no objects with intermediate misalignments ($|\theta_{VLBI} - \theta_{arcsec}| < 70°$). This relationship between maximum polarization and misalignment is significant at the 99% confidence level. In this particular plot we use maximum polarization rather than the first measured value, because that allows the addition of the Rusk data set. Earlier in the paper, it was pointed out that p_1 and p_{max} are strongly correlated. Figure 12 shows the data for the VLBI sample (*filled symbols*), and for a larger but inhomogeneous sample of radio sources (*open symbols*). For the two samples combined, the probability that misalignment and p_{max} are not related is only 2×10^{-4}. It is striking that none of the sources with $p_{max} > 22\%$ has $|\theta_{VLBI} - \theta_{arcsec}| < 50°$.

The distributions of $|\theta_{VLBI} - \theta_{arcsec}|$ are dramatically different for high- and low-polarization objects. For low-polarization objects the distribution is broadly peaked around zero, while for high-polarization objects the distribution is split

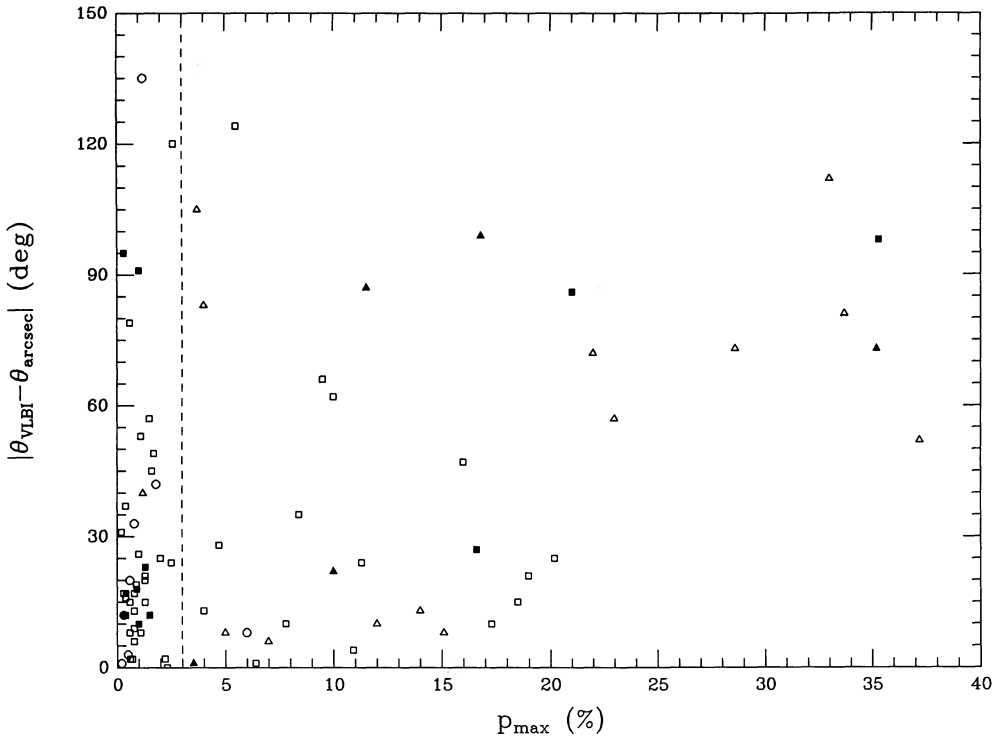

FIG. 12.—Bend angle between the axis of arcsecond and milliarcsecond radio structure plotted against maximum optical polarization. Circles are radio galaxies, squares are strong-lined objects, and triangles are weak-lined objects. Filled symbols are sources from the VLBI sample, open symbols are sources from Rusk (1988). The misalignments are taken from Pearson & Readhead (1988) and Rusk (1988), and the values of p_{max} comes from the references to Table 1 in this paper. For sources with misalignments given by both Pearson & Readhead and by Rusk, the values of Pearson & Readhead were used; otherwise, no attempt has been made to determine misalignments consistently for all objects.

into two peaks, one around 0°, the other around 90°. When the sources with high polarization are subdivided according to the equivalent width of their emission lines, most of the large misalignments come from sources with weak lines. Whereas 11 out of the 18 highly polarized weak-lined objects have $|\theta_{VLBI} - \theta_{arcsec}| > 50°$, only five of the 18 highly polarized strong-lined objects have $|\theta_{VLBI} - \theta_{arcsec}| > 50°$. This separation is significant at the 95% confidence level. The peak in misalignments near 90° was first noted by Pearson & Readhead (1988) in the VLBI sample. The fact that a similar distribution was not seen by Rusk & Rusk (1986) is accounted for by the fact that while neither group divided the sources according to optical polarization, there are many steep spectrum, low-polarization quasars with intermediate misalignments in the Rusk sample, but none in the VLBI sample. Although determination of $|\theta_{VLBI} - \theta_{arcsec}|$ is complicated by many factors, as discussed by Pearson & Readhead (1988), such factors would almost certainly tend to smear out the distribution for the highly polarized sources, rather than make it bimodal as shown in Figure 12. A careful analysis of misalignments for a large sample of highly polarized sources is clearly required.

6. THE ROLE OF RELATIVISTIC BEAMING

The arguments for bulk relativistic motion in compact radio sources were summarized in § 1. The "standard model" to explain the apparently superluminal motions of radio source components is based on an idea first put forward by Rees (1967). Radiating blobs or plasmons move at velocities close to c, and an observer whose line of sight is nearly aligned with the motion sees large apparent transverse velocities and radiation that is amplified by relativistic aberration (Pearson & Zensus 1987). Superluminal motion and Doppler boosting are correlated in strong radio sources, which is an argument in favor of the standard ballistic model, and against light-echo and dipole models (Cohen et al. 1988). However, realistic beaming models differ in three important ways from the standard model. First, the relationship between the opening angle of the beamed emission and the Lorentz factor may not be a simple one (Lind & Blandford 1985; Ghisellini & Maraschi 1989). The parent (or misaligned) population is often identified based on a half angle to the beaming cone of $\theta \sim 1/\gamma$, but it is possible to have beam emission both broader and narrower than $1/\gamma$. Second, the velocity of the radiating material may not be the same as the velocity inferred from apparent superluminal motion. In a nonsteady flow where the emission arises behind strong shocks, the effective Lorentz factor for beaming might be only half that inferred from the superluminal motion (Peacock 1987). Third, the interpretation of the VLBI data requires a *distribution* of Lorentz factors (Cohen 1989).

6.1. *Beamed Optical and Radio Emission*

In § 5 we supposed that quasar optical emission comprises a relatively steady, unpolarized component and a highly variable, highly polarized component. Given that most superluminal sources show blazar activity, that relativistic motion is well established in superluminal sources (Cohen 1989), that beaming is an inevitable consequence of relativistic motion, and that blazar activity is *never* seen in radio-quiet quasars, it is natural to suppose that the polarized optical synchrotron emission is directly related to the radio synchrotron component.

The conditions for self-absorption in a synchrotron plasma

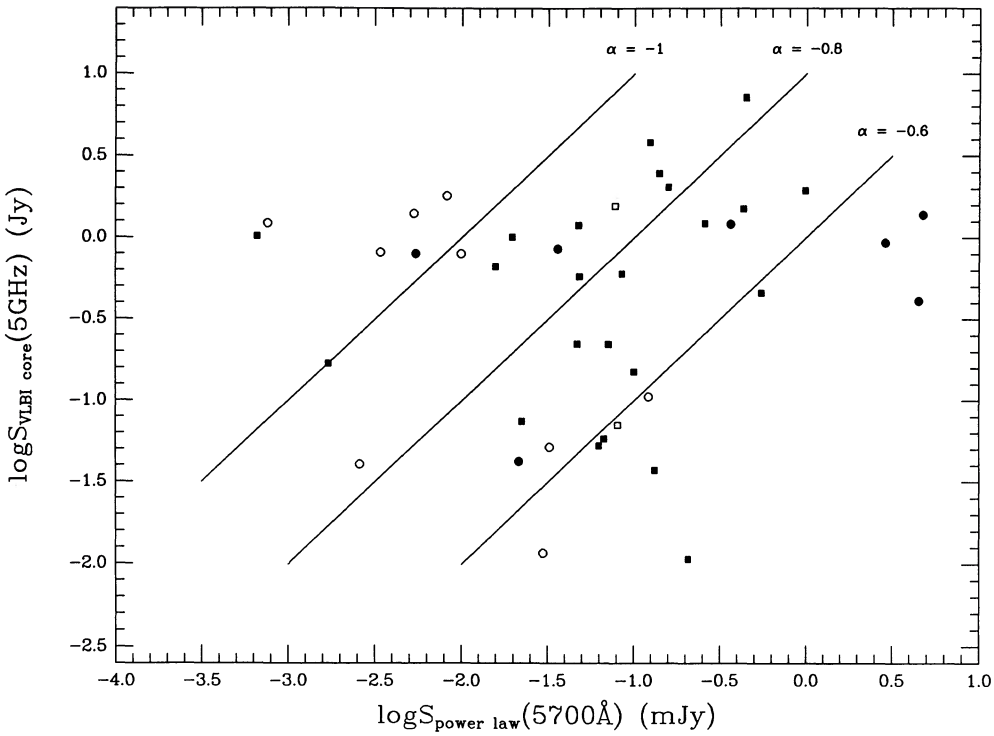

FIG. 13.—Flux density of an optical power-law component at 5700 Å vs. 5 GHz flux density in the VLBI core (Pearson & Readhead 1988). Lines of constant radio-to-optical spectral index are shown. Meaning of symbols is the same as in Fig. 1.

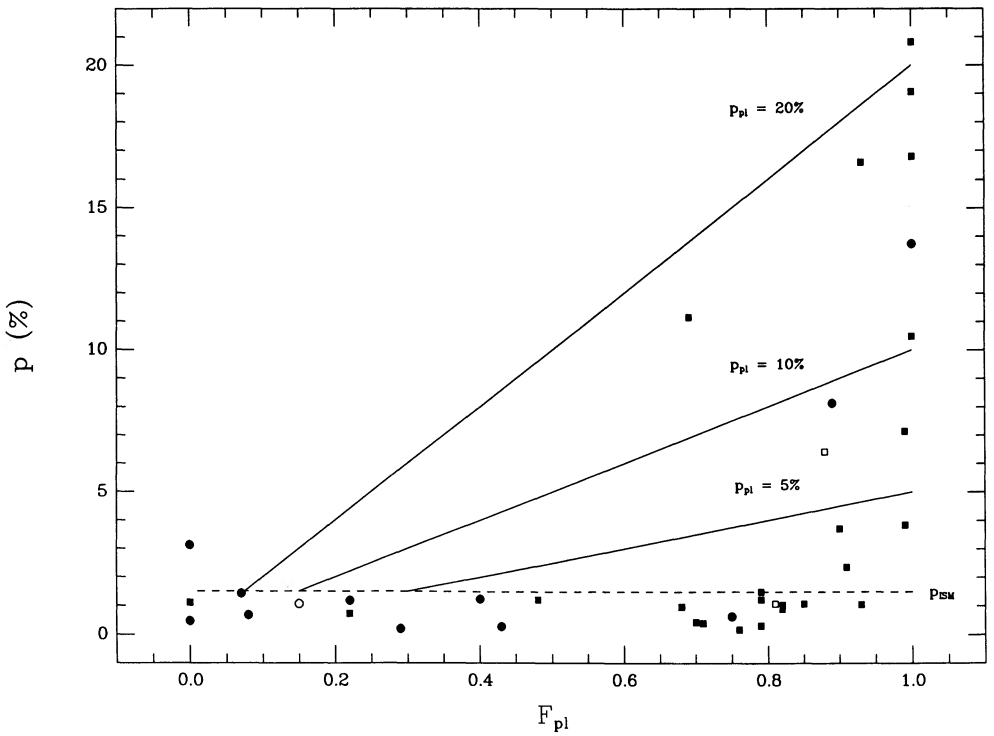

FIG. 14.—Optical polarization vs. the fraction of optical flux density in a power-law component at 5700 Å. Solid lines show different values of the intrinsic power-law polarization; the dashed line is the envelope of values of interstellar polarization. Symbols as in Fig. 1.

depend on frequency, so optical and radio synchrotron emission may come from different regions. Figure 13 shows little relationship between the flux density of the VLBI core and the flux of any power-law component in the MINIPOL bandpass, as determined by simultaneous fitting of line and continuum components of the spectra. On the other hand, if an optical synchrotron component is the source of the polarization, there should be a close (but not necessarily simple) relationship between the polarization and the fraction of the optical emission that comes from a power-law component. Figure 14 shows the optical polarization percentage versus the fraction of optical continuum in a power-law component for the sample. The previously discussed relationship between high polarization and radio compactness is reflected in Figure 14, because the objects with large continuum fractions also have compact radio cores. The solid curves show the polarization that would be observed assuming different values of the intrinsic power-law polarization. The dashed line indicates the upper envelope of the distribution of interstellar polarization values for the VLB sample. The calculation of an intrinsic power-law polarization is not reliable below this level, because of contamination by interstellar polarization, and because of the low significance level of polarization measured below 1.5%.

Except for Mrk 501, no object has high polarization without also having a power-law component dominating the optical continuum. Power-law polarizations in the range 5%–20% could have been detected for sources with relatively weak power laws ($0.3 < F_{pl} < 0.85$), yet only one source in this range has a high measured polarization. We will return to this point later. The nonsimultaneity of the ordinate and abscissa could have a significant effect on Figure 14. In particular, Mrk 501 is a known optical variable with an amplitude of 0.9 mag (Pica et al. 1988), so the power-law fraction undoubtedly changes with epoch. Thus we conclude that a strong power-law component is a necessary, but not a sufficient condition, for high optical polarization in active nuclei.

The highest redshift objects in this sample and others tend to be unpolarized (Stockman, Moore, & Angel 1984; Fugmann & Meisenheimer 1988; Wills 1989), due to the fact that we observe high-redshift objects at short rest wavelengths, where red power-law components are weak. For example, the low-polarization object 0212+735, at $z = 2.367$, has essentially no power-law contribution in the MINIPOL bandpass, although its spectrum is dominated by blackbody and Balmer continuum components that result in low equivalent widths for the lines. Thus high polarization in high-redshift quasars will be found in the infrared, if it is found at all.

This is reflected in Figure 15, which shows the redshift distributions of sources from the VLBI sample (quasars and radio galaxies) and the complete 5 GHz sample of Impey & Tapia (1990; quasars) combined. The three panels show high-polarization quasars, low-polarization quasars, and sources with both weak lines and high polarization (only one out of 180 sources has both weak lines *and* low polarization). The bottom panel includes classical BL Lac objects. The redshift distribution of the weak-lined sources is different from that of the high- and low-polarization quasars at the 93% and 97% confidence levels, respectively. There is a small but noticeable difference between the redshift distributions of the high and low polarization quasars (see also Wills 1989). The fraction of quasars with high polarization falls from 0.43 ± 0.09 ($0 < z < 1$) to 0.36 ± 0.10 ($1 < z < 2$) to 0.22 ± 0.15 ($2 < z < 3$). The spectral decomposition of Wills (1989) can be

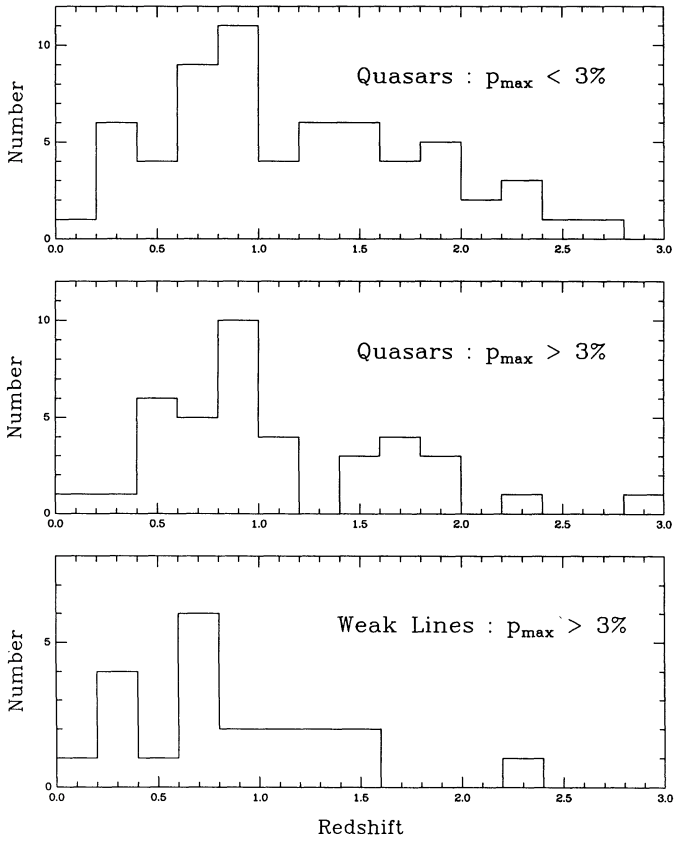

FIG. 15.—Redshift distributions for the objects in the VLBI sample plus the complete 5 GHz sample of quasars in Impey & Tapia (1989), divided into high- and low-polarization quasars and highly polarized weak-lined objects. Only one out of 180 sources in the combined sample had both weak lines and low polarization.

used to calculate the decrease in detectivity of a polarized power law as redshift increases. Assuming $p_{max} = 30\%$, the net polarization of the power law plus blue bump drops below the detection threshold of 3% around $z = 1.8$, as observed. The efficiency of detecting high polarization (assuming p uniformly distributed between 0 and p_{max}, and normalizing to $z = 0$) falls from 0.59 ($0 < z < 1$) to 0.35 ($1 < z < 2$) to 0.21 ($2 < z < 3$). When this selection effect is accounted for, the redshift distributions of high- and low-polarization quasars are indistinguishable. We will discuss the difference between the redshift distributions of strong- and weak-lined objects in § 6.3.

Figure 16 shows the relationship between three optical indicators of synchrotron emission and the VLBI compactness F_c. The main feature of the observations is a sudden appearance of high polarization values, high power-law fractions, and low-contrast emission lines, all occurring at a value of $F_c \sim 0.3$. We have previously remarked on the fact that polarizations in the range 5%–20% could have been detected for sources with $0.3 < F_{pl} < 0.85$, yet only one source in this range has a high measured polarization. This can be seen in a comparison of the top and bottom panels of Figure 16: objects with $-1.6 < \log F_c < -0.5$ sometimes have large power-law fractions, but not high polarizations. To try to account for the difference between the top and bottom panels of Figure 15, we assumed that the distribution of p for the 10 objects in the sample with $F_c > 0.9$ represented the intrinsic distribution of p for power-law components in general. The power-law fraction for each

object in the bottom panel was then multiplied by those 10 values of p, giving a simulated set of measurements of p and F_c for a sample 10 times as large. Many 10% subsets of the objects in the supersample were then selected randomly, plotted as in the upper panel of Figure 16, and compared with that panel. In $\sim\frac{1}{3}$ of the cases, the qualitative appearance of the two plots was the same, with almost no objects with $-1.6 < \log F_c < -0.5$ having polarizations above 5%. We conclude, therefore, that the dearth of high-polarization objects with intermediate power-law fractions is due to a combination of the underlying distribution of power-law polarizations and the small number of sources with intermediate power-law fractions.

The curves on Figure 16 represent the predictions of a beaming model with an isotropic component with flux density $S_{\rm iso}$, and a relativistically moving component with flux density at an angle θ to the direction of motion of $S_\theta = S_T(1-\beta\cos\theta)^{-(2-\alpha)}$, where S_T is $S_\theta(\theta = 90°)$. We define $R \equiv S_\theta/S_{\rm iso}$, $R_T \equiv S_T/S_{\rm iso}$, and the "amplification" of the moving component $A \equiv S_\theta/S_T$. These expressions are applied to both radio and optical emission, with $\alpha_{\rm rad} = 0.0$ and $\alpha_{\rm opt} = -0.7$. The optical boosting is therefore related to the radio boosting, which is given by the observables F_c and $R_T^{\rm rad}$. Following Orr & Browne (1982), we assume $R_T^{\rm rad} = 0.01$. If we normalize the flux density of the isotropic optical component to unity, the only other free parameter is the ratio of the transverse optical jet to the isotropic optical component, $R_T^{\rm opt}$. For the model, we assume a power-law polarization of 20% and a ratio of line to unbeamed continuum of 15.

Figure 16 shows the upper envelopes of p, L/C, and $F_{\rm pl}$, as given by this model for different values of $R_T^{\rm opt}$. In terms of A and $R_T^{\rm opt}$, $F_{\rm pl} \approx p \approx 1/(1 + 1/AR_T^{\rm opt})$, and $L/C \approx 1/(1 + AR_T^{\rm opt})$. This amplitude of optical flux variability will scale the same

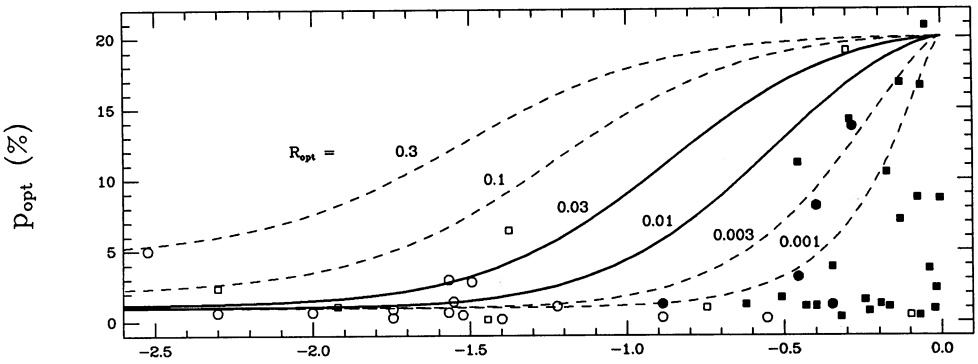

FIG. 16a

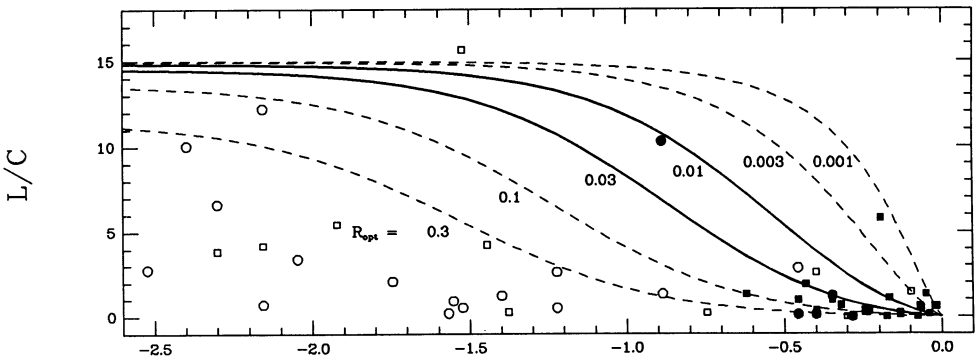

FIG. 16b

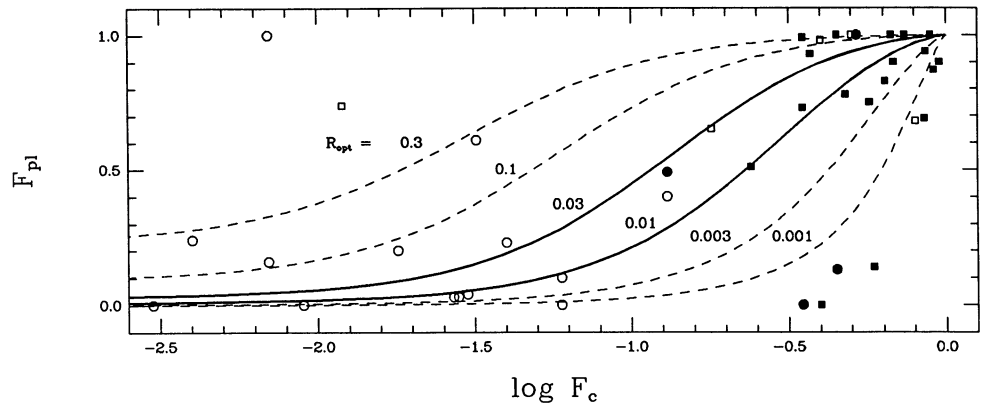

FIG. 16c

FIG. 16.—Radio core fraction F_c vs. (*a*) optical polarization, (*b*) line-to-continuum ratio, and (*c*) fraction of the optical continuum which is a power law. The curves represent a model with the same beaming cone used for the radio and optical emission, for various values of $R_T^{\rm opt}$, the ratio of beamed to isotropic optical emission transverse to the jet direction. The symbols are as in Fig. 1.

way as p and F_{pl}, and we have already noted that polarization and flux variability scale similarly with F_c in this sample. In the bottom panel of Figure 16, we omit four sources which do not have reliable values of F_c published by Pearson & Readhead (1988). The upper envelope of the data fixes the isotropic optical component to be in the range $0.01 < R_T^{opt} < 0.1$. Because of the dependence of A on spectral index, the optical amplification for a given value of θ and γ will be larger than the radio amplification. This should translate into a dependence of radio-to-optical spectral index, α_{ro} on F_c. For sources with weak lines and high polarizations (including the classical BL Lac objects), $F_c = 0.62 \pm 0.19$, compared with 0.30 ± 0.31 for low-polarization quasars (the difference is significant at the 95% confidence level). The beam model predicts that $(\alpha_{ro})_{F_c > 0.5} = (\alpha_{ro})_{F_c < 0.1} + 0.14$. We observe $(\alpha_{ro})_{BL\ Lac} = (\alpha_{ro})_{quasar} + 0.15$, in close agreement.

These results strongly support the idea that compact radio sources have beamed optical radiation. Four indicators of optical synchrotron emission are all closely correlated with radio compactness: polarization, power-law fraction, line-to-continuum ratio, and amplitude of flux variability. Moreover, the data are consistent with a simple model of Doppler boosting, where the radio and optical emitting regions have the same beaming cone. Amplification of a factor of 10–100 is required before the beam synchrotron component dominates the isotropic (unpolarized, quiescent) component. A similar model has been successfully applied to 3C 273, where the amplification is not sufficient for the blazar component to dominate the optical emission (Impey, Malkan, & Tapia 1989). It is natural to identify the isotropic optical component with the quiescent and unpolarized continuum seen in most steep spectrum quasars.

Our conclusion that the radio and optical emitting regions have the same beaming geometry is not necessarily in conflict with Ghisellini & Maraschi (1989), who concluded that X-rays were beamed into a wider cone than radio emission. We have only to suppose that collimation of the jet is completed between the region from which the X-rays emerge and the region from which the optical synchrotron emission comes, after which the beaming geometry remains relatively constant.

6.2. *Constraints on Beaming Models*

A logical extension of existing beaming models is to assume a distribution of Lorentz factors for the relativistic flow. This is in fact required by the VLBI data (Cohen 1989). As pointed out by Peacock (1987), invoking a distribution of Lorentz factors allows a small fraction of the randomly oriented population to have very large amplifications without producing large numbers of core-dominated sources. Cohen (1989) has calculated the expected distribution of superluminal velocities in the ballistic model for one-sided jets. For any reasonable shape of the luminosity function, the distribution peaks up at the highest velocities. More than 50% of the sources will have $v > 0.8v_{max}$. By contrast, the observed distribution of apparent v/c peaks at low velocities. Figure 17 shows the histogram of v/c for 33 objects from Cohen (1989), where the dashed and solid curves are plotted for a fixed value of γ and distributions of γ, respectively (assuming $\gamma_{max} = 10$). Distributions where large Lorentz factors are rarer than small Lorentz factors provide a good fit to the data.

If the Orr & Browne (1982) scheme is correct, the luminosity functions of flat and steep spectrum quasars provide more evidence for a distribution of Lorentz factors. Orr & Brown argued that steep spectrum quasars were the parent population of the beamed flat spectrum quasars. Peacock (1987) has shown that the ratio of space densities of flat and steep spec-

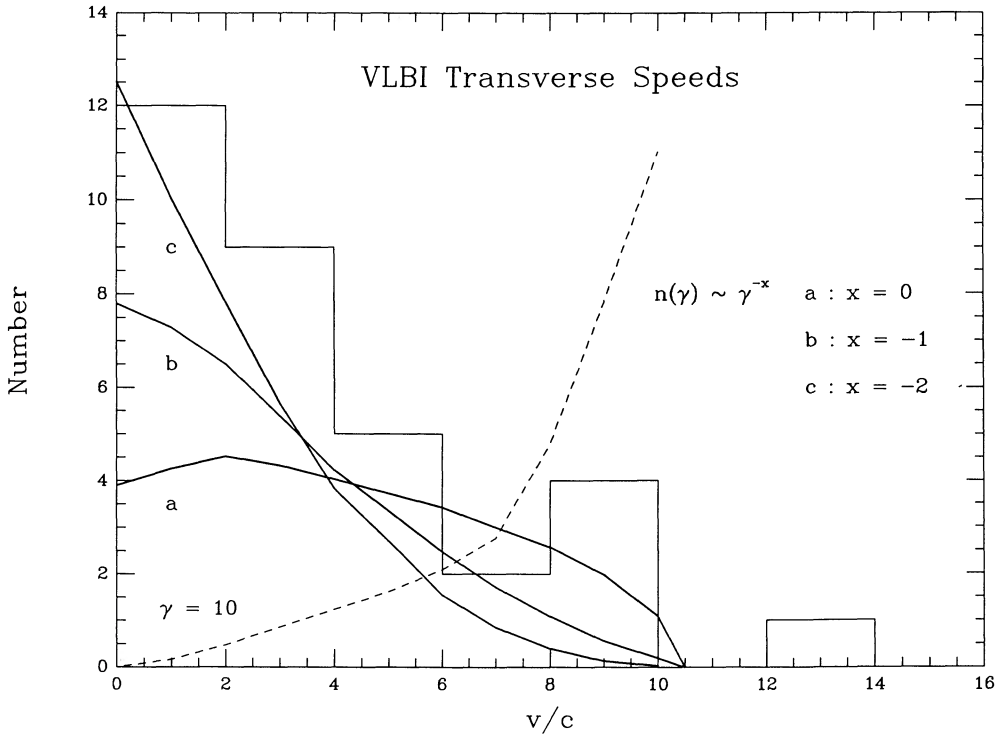

FIG. 17.—Histogram of observed values of v/c from Cohen (1989). The dashed curve is for $\gamma = 10$, and the solid curves are for distributions $f(\gamma) \sim \gamma^x$, where $x = 0, -1, -2$.

trum quasars is given by $\rho_{fs}/\rho_{ss} \approx [(1-\beta)/\beta][A_{max}^{\delta}/\delta(2+\alpha)]$, where $N(>L) \sim L^{-\delta}$, $\delta \approx 1.5$, and A_{max} is the amplification of the *total* flux density (beamed plus isotropic) at $\theta = 0°$ relative to $\theta = 90°$. Observed luminosity functions give $\rho_{fs}/\rho_{ss} \approx 1$ at $z = 1$. Since $\rho_{fs}/\rho_{ss} \propto \gamma^6$, Peacock points out that ρ_{fs}/ρ_{ss} depends on the *maximum* value of γ for the model. A single value of $\gamma_{max} \sim 10$ gives $\rho_{fs}/\rho_{ss} = 13.8$, which is too high. However, a model with a distribution of Lorentz factors such as $f(\gamma) \sim \gamma^x$ gives $\rho_{fs}/\rho_{ss} = 3.8$, 2.2, or 1.0 for $x = 0, -1$, or -2. Therefore, the Orr & Browne scheme is only consistent with the observed value of γ_{max} if $x \sim -2$.

6.3. *A Cow is Not a Horse of a Different Color*

We have shown that the strong correlations in the VLBI sample between high polarization, weak emission lines (i.e., lines of small equivalent width), and radio compactness can be accounted for by a simple model in which the strength of a beamed optical synchrotron component is directly related to the radio core strength and subject to the same beaming geometry. We emphasize that this result applies to the entire VLBI sample (more precisely, the 50 sources that we measured), which, unlike previous polarization studies, includes galaxies as well as quasars. It is time now to consider differences, rather than similarities, between various sources. To anticipate the conclusion, we will argue that highly polarized sources with weak emission lines are of two types, high-luminosity objects like "normal" quasars overwhelmed by a strongly beamed continuum, and low-luminosity objects like BL Lacertae overwhelmed by a modestly beamed continuum.

The extended radio power P_{ext} (in W Hz^{-1} sr^{-1}) at 1.4 GHz of classical BL Lac objects generally lies in the range $21.5 < \log P_{ext} < 24.5$, corresponding to F-R I radio galaxies (Orr & Browne 1982). (In terms of L_{320} in Table 2, the division between F-R I and F-R II galaxies occurs at $\sim 10^{25}$ W Hz^{-1} sr^{-1}). On the other hand both high- and low-polarization quasars have $24 < \log P_{ext} < 27$, corresponding to F-R II radio galaxies. The few weak-lined sources at high redshift have F-R II extended luminosities. Extended radio emission is isotropic. Narrow-line emission in radio sources may be somewhat anisotropic, but the variation in apparent luminosity with orientation appears to be a factor of 10 or less (Jackson et al. 1989; Lawrence 1990). Emission-line luminosities for classical BL Lac objects lie in the range $31.4 < \log L_{[O\ III]} < 34.4$, whereas for both high- and low-polarization quasars they lie in the range $34.4 < \log L_{[O\ III]} < 35.9$ (Stickel, Fried, & Kühr 1989a; Jackson et al. 1989). Narrow-line luminosity therefore seems to scale with extended radio luminosity in blazars just as it does in radio galaxies (McCarthy 1988; Rawlings et al. 1989; Baum & Heckman 1989). In terms of extended radio and narrow-line luminosity some weak-lined objects are like quasars and F-R II galaxies, while some are like F-R I galaxies. In addition, there are differences in spectral parameters. The synchrotron power law in high-polarization quasars has a slope of $\alpha_{opt} \sim -2$ (Wills 1989), considerably steeper than the power-law slope in classical BL Lac objects, $\alpha_{opt} \sim -1.4$ (Impey & Neugebauer 1988). Also, Worrall (1989) has shown that the X-ray slopes of both high- and low-polarization quasars are $\alpha_{X\text{-}ray} = -1$, whereas the classical BL Lac objects have flatter slopes, $\alpha_{X\text{-}ray} = -0.5$.

There is a clear difference between the distributions of v/c for sources with strong and weak emission lines. While sources with strong lines are found at all values of v/c, if we accept the unconfirmed redshifts of $z = 0.77$ for 1749+701 and $z = 0.342$ for 2007+777 from Stickel, Fried, & Kühr (1989b), then all six weak-lined objects with measured values of v/c have $v/c < 4$. This suggests that the weak-lined objects either have large values of γ but are oriented very close to the line of sight or have relatively small values of γ. We will consider these two possibilities in turn.

Transverse speed reaches its maximum of $\sim\gamma$ when $\theta \approx 1/\gamma$. Thus the fastest quasars, with $\gamma \approx 10$, would have $\theta \approx 6°$, and objects with $v/c \approx 4$ would have $\theta \approx 1°$. Extra Doppler boosting at the smaller angle would be a factor of 3.7 at radio wavelengths and 5.6 at optical wavelengths, and would reduce the equivalent width of emission lines by the same factor. Thus objects with angles to the line of sight $\theta \ll 1/\gamma$ would be weak lined. The simple beaming model of the previous section predicts $F_c = 0.50$ for the quasars and $F_c = 0.78$ for the weak-lined objects. In the VLBI sample, we find $F_c = 0.47 \pm 0.31$ for quasars and $F_c = 0.70 \pm 0.06$ for weak-lined objects. In a flux-limited sample at high frequencies where beamed emission can dominate, the small angle hypothesis predicts that 4%–13% of the sources will be weak-lined objects with slow speeds, the exact percentage depending on the slope of the luminosity function (Cohen 1989). In the VLBI sample 15% of the sources have weak emission lines ($L/C < 0.2$). In an orientation-unbiased sample selected at low frequencies, on the other hand, the beaming cone is so small that one would expect less than 1% weak-lined objects. Only one out of the 168 3CR sources is a weak lined object (3C 66A), consistent with this prediction. All but one of the weak-lined objects with measured v/c is a luminous source with $z > 0.1$, and extended radio luminosity in the F-R II range. All of this is consistent with the hypothesis that high-luminosity weak-lined objects are a closely aligned subset of the quasar population.

Suppose instead that $\gamma_{max} \approx 4$. The fastest weak-lined objects would have $\theta = 14°.3$, the maximum optical amplification would be 130 times smaller than for $\gamma = 10$, and the radio core fraction would be correspondingly lower. However, a modestly Doppler-boosted continuum may dominate low-luminosity lines just as well as a strongly boosted continuum dominates high-luminosity lines (Lawrence 1990), and the required emission line luminosity is comparable to that of low-luminosity F-R I galaxies. In the VLBI sample BL Lacertae itself shows just this combination of small v/c with low line and radio luminosities. About 6% of an orientation unbiased sample would have $\theta < 14°$. We conclude that weak-lined objects have low speeds for two separate reasons, small θ in the high-luminosity objects and low γ in the low-luminosity, classical BL Lac objects.

This conclusion is supported by the radio and line luminosity data previously discussed. The classical BL Lac objects observed at low redshift embedded in elliptical galaxies are thus physically distinct from the weak-lined, luminous sources seen at high redshift (Browne 1989). The redshift distributions of strong- and weak-lined sources shown in Figure 15 are also consistent with this interpretation. Moreover, if the parent populations of BL Lac objects and highly polarized quasars are F-R I radio galaxies and steep spectrum quasars, respectively, then BL Lac objects would be expected to show far less cosmic evolution than highly polarized quasars. This would bring the properties of radio and X-ray–selected BL Lac objects into closer accord (Maccacaro et al. 1989).

7. SUMMARY

We have measured the optical polarization of 50 sources out of 65 in a complete sample selected at 5 GHz. This sample has been the subject of a multi-epoch campaign of very long

baseline interferometry, and is the first sample with extensive information on milliarcsecond radio structure, optical spectroscopy, and optical polarization. The sample is almost equally divided into radio galaxies and quasars. We conclude the following:

1. High polarization ($p > 3\%$) is strongly correlated with the fraction of the total 5 GHz flux density found in a milliarcsecond core (F_c), and with the fraction of optical emission found in a power-law continuum. The fraction of sources with high polarization rises from 13% for sources with $F_c < 0.1$ to 45% for sources with $F_c > 0.1$. Essentially every radio source with all of its flux density in an unresolved milliarcsecond core is highly polarized. Two thirds of the known superluminal sources in the sample have high polarization.

2. Few radio galaxies contain optical cores with high polarization. However, assuming that the synchrotron power law is diluted by starlight from a giant elliptical galaxy, the detection rate of such cores is consistent with the hypothesis that *all* radio sources contain optically polarized cores, with strength proportional to the core radio flux density. The quasars in the sample have predominantly compact radio emission, and high polarization is correspondingly more common. A minimum of 60% of quasars selected at 5 GHz have $p_{\max} > 3\%$, when a simple correction for the duty cycle of high- and low-polarization states is made.

3. High optical polarization, optical power-law fraction, line-to-continuum ratio, emission lines of small equivalent width, and large amplitude flux variability are all strongly corrected with the fraction of the 5 GHz radio flux density that is unresolved on VLBI scales. The distributions of these optical properties are well matched by a model where the radio and optical radiation have the same beaming geometry. Optical beaming of a factor of 10–100 is required before a radio source shows blazar properties.

4. We confirm in this complete sample a striking alignment of the position angle of the VLBI structure axis and the position angle of optical polarization in highly polarized sources. Low-polarization sources do not show the same alignment. We also find that the highly polarized sources have a large amount of *mis*alignment between the VLBI structure axis and the axis of large-scale radio structure. The largest misalignments are observed for sources with high polarization *and* weak emission lines.

5. Combining this sample with another complete quasar sample, we find that the redshift distributions of high- and low-polarization quasars are similar. The small deficit of highly polarized quasars at high redshifts can be understood in terms of a red power law diluted with a blue thermal component, such that the power law is less prominent in the observed frame at high redshift.

6. The properties of weak-lined objects are consistent with the hypothesis that such objects are either (*a*) sources of high low-frequency-radio and line luminosity and large γ, viewed at such a small angle to the line of sight that a highly beamed continuum outshines strong emission lines; or (*b*) sources of low low-frequency-radio and line luminosity and moderate γ, viewed at $\sim 1/\gamma$ to the line of sight, so that a modestly beamed continuum outshines weak emission lines. If the unbeamed parent population of the high-luminosity source is powerful F-R II radio galaxies, the parent population of the low luminosity sources (i.e., classical BL Lac objects) is F-R I galaxies.

7. Various properties of core dominated radio samples require a beaming model with a range of Lorentz factors, with higher values less common. If $f(\gamma) \sim \gamma^x$, where $-2 < x < -1$, then the beaming model can be made consistent with: (*a*) the observed distribution of v/c; (*b*) the space densities of steep and flat spectrum quasars in the Orr and Browne unified scheme; and (*c*) the rarity of sources with high Doppler boosting in core-dominated samples.

We thank Richard Young at Steward Observatory for building the device that was used to adapt MINIPOL to the Palomar 200 inch (5 m) telescope, and we thank the mountain crew at Palomar Observatory for their assistance. Juan Carrasco was our excellent telescope operator for these observations. C. D. I. is grateful to Caltech for a Weingart Fellowship and acknowledges support from NSF grant AST-8700741 and NASA/JPL contract 958028. C. R. L. acknowledges support from NSF grant AST-8814554. S. T. was supported in part by NASA grant INT 82-13103 and grant CW 0006-85 from the Space Telescope Science Institute.

REFERENCES

Alighieri, S., Fosbury, R. A. E., Quinn, P. J., & Tadhunter, C. N. 1990, Nature, 341, 307
Aller, H. D., Aller, M. F., & Hughes, P. A. 1985, ApJ, 298, 296
Aller, H. D., Hughes, P. A., & Aller, M. F. 1987, in Superluminal Radio Sources, ed. J. A. Zensus & T. J. Pearson (Cambridge: Cambridge University Press), p. 273
Angel, J. R. P., et al. 1978, in Proc. Pittsburgh Conf. on BL Lac Objects, ed. A. M. Wolfe (Pittsburgh: University of Pittsburgh Press), p. 117
Angel, J. R. P., & Stockman, H. S. 1980, ARA&A, 18, 321
Antonucci, R. R. J. 1983, Nature, 303, 158
———. 1984, ApJ, 278, 499
Barthel, P. D. 1989, ApJ, 336, 606
Baum, S. A., & Heckman, T. M. 1989, ApJ, 336, 702
Biermann, P., et al. 1981, ApJ, 247, L53
Blandford, R. D., & Königl, A. 1979, ApJ, 232, 34
Blandford, R. D., & Rees, M. J. 1978, in Proc. Pittsburgh Conf. on BL Lac Objects, ed. A. M. Wolfe (Pittsburgh: University of Pittsburgh Press), p. 328
Browne, I. W. A. 1989, in BL Lac Objects, ed. L. Maraschi, T. Maccacaro, & M.-H. Ulrich (Berlin: Springer-Verlag), p. 401
Cawthorne, T. V., & Wardle, J. F. C. 1988, ApJ, 332, 696
Cohen, M. H. 1989, in BL Lac Objects, ed. L. Maraschi, T. Maccacaro, & M.-H. Ulrich (Berlin: Springer-Verlag), p. 13
Cohen, M. H., Barthel, P. D., Pearson, T. J., & Zensus, J. A. 1988, ApJ, 329, 1
Dolan, J. F., & Tapia, S. 1986, PASP, 98, 792
Fugmann, W., & Meisenheimer, K. 1988, A&A, 207, 211.
Gabuzda, D. C., Cawthorne, T. V., Roberts, D. H., & Wardle, J. F. C. 1989, in BL Lac Objects, ed. L. Maraschi, T. Maccacaro, & M.-H. Ulrich (Berlin: Springer-Verlag), p. 22
Gabuzda, D. C., Wardle, J. F. C., & Roberts, D. H. 1989, ApJ, 336, L59
Ghisellini, G., & Maraschi, L. 1989, ApJ, 340, 181
Hutchings, J. B. 1987, ApJ, 320, 122
Impey, C. D. 1987, in Superluminal Radio Sources, ed. J. A. Zensus & T. J. Pearson (Cambridge: Cambridge University Press), p. 233
Impey, C. D., Brand, P. W. J. L., Wolstencroft, R. D., & Williams, P. M. 1982, MNRAS, 209, 245
Impey, C. D., Malkan, M. A., & Tapia, S. 1989, ApJ, 347, 145
Impey, C. D., & Neugebauer, G. 1988, AJ, 95, 307
Impey, C. D., & Tapia, S. 1988, ApJ, 333, 666
———. 1990, ApJ, 354, 124
Jackson, N., Browne, I. W. A., Murphy, D. W., & Saikia, D. J. 1989, Nature, 338, 485
Jannuzi, B., & Elston, R. 1991, ApJ, 366, 69
Jones, T. W. 1988, ApJ, 332, 768
Kellermann, K. I., & Pauliny-Toth, I. I. K. 1981, ARA&A, 19, 373
Kormendy, J. 1986, in Nearly Normal Galaxies from the Planck Time to the Present, ed. S. M. Faber (New York: Springer-Verlag), p. 163
Kühr, H., & Schmidt, G. D. 1989, AJ, 99, 1
Landau, R., et al. 1986, ApJ, 308, 78
Lawrence, C. R. 1990, in Parsec-Scale Radio Jets, ed. A. Zensus & T. J. Pearson (Cambridge: Cambridge University Press), p. 280

Lawrence, C. R., Pearson, T. J., Readhead, A. C. S., & Unwin, S. C. 1986, AJ, 91, 494
Lawrence, C. R., Readhead, A. C. S., Pearson, T. J., & Unwin, S. C. 1987, in Superluminal Radio Sources, ed. J. A. Zensus & T. J. Pearson (Cambridge: Cambridge University Press), p. 260
Lilly, S. J., McLean, I. S., & Longair, M. S. 1984, MNRAS, 209, 401
Lind, K., & Blandford, R. D. 1985, ApJ, 295, 358
Linfield, R. P., et al. 1989, ApJ, 336, 1105
Maccacaro, T., Gioia, I. M., Schold, R. E., Wolter, A., Morris, S. L., & Stocke, J. T. 1989, in BL Lac Objects, ed. L. Maraschi, T. Maccacaro, & M.-H. Ulrich (Berlin: Springer-Verlag), p. 222
Marscher, A. P., Marshall, R. E., Mushotzsky, R. F., Dent, W. A., Balonek, T. A., & Hartman, M. F. 1979, ApJ, 233, 498
Maza, J. 1979, Ph.D. thesis, University of Toronto
McCarthy, P. M. 1988, Ph.D. thesis, University of California at Berkeley
Miley, G. K. 1980, ARA&A, 18, 165
Miller, J. S. 1975, ApJ, 200, L55
Miller, J. S., & French, H. B. 1978, in Proc. Pittsburgh Conf. on BL Lac Objects, ed. A. M. Wolfe (Pittsburgh: University of Pittsburgh Press), p. 228
Moore, R. L., & Stockman, H. S. 1981, ApJ, 243, 60
———. 1984, ApJ, 279, 465
Orr, M. J. L., & Browne, I. W. A. 1982, MNRAS, 200, 1067
Owen, F. N. 1986, in IAU Symposium 119, Quasars, ed. G. Swarup & V. J. Kapahi (Dordrecht: Reidel), p. 173
Peacock, J. A. 1987, in Astrophysical Jets and Their Engines, ed. W. Kundt (Dordrecht: Reidel), 185
Pearson, T. J., & Readhead, A. C. S. 1981, ApJ, 248, 61
———. 1988, ApJ, 328, 114
Pearson, T. J., & Zensus, J. A. 1987, in Superluminal Radio Sources, ed. J. A. Zensus & T. J. Pearson (Cambridge: Cambridge University Press), p. 1
Phinney, E. S. 1985, in Astrophysics of Active Galaxies and Quasi-Stellar Objects, ed. J. Miller (Mill Valley: University Science Books), p. 455
Pica, A. J., Smith, A. G., Webb, J. R., Leacock, R. J., Clements, S., & Gombola, P. P. 1988, AJ, 96, 1215
Preston, R. A., Morabito, D. D., Williams, J. G., Faulkner, J., Jauncey, D. L., & Nicolson, G. D. 1985, AJ, 90, 1599
Quirrenbach, A., & Witzel, A. 1990, A&A, in press
Rawlings, S., Saunders, S., Eales, S. A., & Mackay, C. D. 1989, MNRAS, 240, 701
Rees, M. J. 1967, MNRAS, 135, 345
Rudy, R. J., Schmidt, G. D., Stockman, H. S., & Moore, R. L. 1983, ApJ, 271, 59
Rusk, R. E. 1988, Ph.D. thesis, University of Toronto
———. 1990, JRAS Canada, 84, 199
Rusk, R. E., & Rusk, A. C. M. 1986, Canadian J. Phys., 64, 440
Rusk, R. E., & Seaquist, E. R. 1985, AJ, 90, 30
Scheuer, P. A. G. 1987, in Superluminal Radio Sources, ed. J. A. Zensus & T. J. Pearson (Cambridge: Cambridge University Press), p. 104
Schneider, D. P., Gunn, J. E., & Hoessel, J. G. 1983, ApJ, 268, 476
Simmons, J. F. L., & Stewart, B. G. 1985, A&A, 142, 100
Sitko, M. L., Schmidt, G. D., & Stein, W. A. 1985, ApJS, 59, 323
Smith, P. S., Balonek, T. J., Elston, R., & Heckert, P. A. 1987, ApJS, 64, 459
Smith, P. S., Balonek, T. J., Heckert, P. A., & Elston, R. 1985, ApJ, 385, 404
Stickel, M., Fried, J. W., & Kühr, H. 1989a, in BL Lac Objects: Ten Years After, ed. L. Maraschi, T. Maccacaro, & M.-H. Ulrich (Berlin: Springer-Verlag), p. 64
———. 1989b, A&AS, 80, 103
Stockman, H. S., Angel, J. R. P., & Miley, G. K. 1979, ApJ, 227, L55
Stockman, H. S., Moore, R. L., & Angel, J. R. P. 1984, ApJ, 279, 485
Tabara, H., & Inoue, M. 1980, A&AS, 39, 379
Ulrich, M.-H. 1989, in BL Lac Objects, ed. L. Maraschi, T. Maccacaro, & M.-H. Ulrich (Berlin: Springer-Verlag), p. 45
Wardle, J. F. C., & Roberts, D. H. 1988, in The Impact of VLBI on Astrophysics and Geophysics, ed. M. J. Reid & J. M. Moran (Dordrecht: Reidel), p. 143
Wardle, J. F. C., Roberts, D. H., Potasch, R. I., & Rogers, A. E. E. 1986, ApJ, 304, L1
Webb, J. R., Smith, A. G., Leacock, R. J., Fitzgibbons, G. L., Gombola, P. P., & Shepherd, D. W. 1988, AJ, 95, 374
Wehrle, A. E., Preston, R. A., Meier, D. L., Gorenstein, M. V., Shapiro, I. I., Rogers, A. E. E., & Rius, A. 1984, ApJ, 284, 519
Wills, B. J. 1989, in BL Lac Objects, ed. L. Maraschi, T. Maccacaro, &. M.-H. Ulrich (Berlin: Springer-Verlag), p. 109
Wills, D., Wills, B. J., Breger, M., & Hsu Jin-Chung. 1980, AJ, 85, 1555
Witzel, A. 1990, in Parsec-Scale Radio Jets, ed. A. Zensus & T. J. Pearson (Cambridge: Cambridge University Press), p. 206
Witzel, A., Schalinski, C. J., Johnston, K. J., Biermann, P. L., Krichbaum, T. P., Hummel, C. A., & Eckart, A. 1988, A&A, 206, 245
Worrall, D. M. 1989, in BL Lac Objects, ed. L. Maraschi, T. Maccacaro, & M.-H. Ulrich (Berlin: Springer-Verlag), p. 305